Performance study of solar photovoltaic-thermal collector for domestic hot water use and thermochemical sorption seasonal storage

Kamon Thinsurat, Huashan Bao*, Zhiwei Ma, Anthony P Roskilly

Sir Joseph Swan Centre for Energy Research, Newcastle University, Newcastle upon Tyne, NE1 7RU, UK

Abstract

To maximise the utilisation of solar energy and improve the solar fraction for domestic applications, this paper explored the potential of the hybrid solar Photovoltaic/Thermal (PV/T) collector integrated with a thermochemical sorption thermal storage system. The thermal output was used to provide domestic hot water or stored over seasons in the England city of Newcastle upon Tyne. The performance of the water-cooled PV/T collectors with or without an air insulation layer between the glass cover and the Photovoltaic (PV) cell was compared. The electrical power generation model of the PV cell developed in MATLAB was coupled with a Computational Fluid Dynamics (CFD) model to simulate the simultaneous generation of electrical and thermal energy. The one-diode model was used to simulate the electrical production of the PV cell with the new correlations of the series resistance and the shunt resistance proposed in this work, so that the accuracy of dynamic performance simulation can be improved especially in the cases with relatively higher PV cell temperature. The water outlet temperature was studied at 100 °C to meet the heat supply requirement of the sorption cycle using the working pair strontium chloride-ammonia. It was found that the PV/T collector with air gap could produce ~~133~~ 28 liter hot water per day per m^2 collector ($L/(day \cdot m^2)$) with the electric efficiency of about 10% if the water outlet temperature was required at 100 °C; in contrast, around ~~28~~ 133 $L/(day \cdot m^2)$ was produced with the electric efficiency of 13% when the water outlet temperature at 40 °C. The PV/T collector without air gap was not competent for the applications studied in this work especially in cold regions. The application case studies suggested that an installation of 26 m^2 air-gap PV/T collectors integrated with the strontium chloride-ammonia thermochemical sorption storage system can fully satisfy the annual hot water demand of an ordinary single household in Newcastle upon Tyne with 100% solar sources, and cover at least half of the annual electricity consumption.

---

* Corresponding author. Tel.: +44 001912084849; Fax: +44 001912226920;
E-mail address: huashan.bao@newcastle.ac.uk

Keywords: solar energy; photovoltaic-thermal collector; domestic hot water use; seasonal thermal energy storage; CFD simulation, thermochemical sorption

Nomenclature

Abbreviations

CFD	computational fluid dynamics
HTF	heat transfer fluid
PCM	Phase change material
PV	photovoltaic
PV/T	photovoltaic/thermal
PV/T-AG	photovoltaic/thermal collector with air gap
PV/T-no-AG	photovoltaic/thermal collector without air gap
STC	standard test condition

Symbols

C_p	specific heat capacity (J/(kg·K))
E_g	band-gap energy of semiconductor used in PV-cell (eV)
g	gravity (m/s^2)
G	solar irradiance (kW/m^2)
Gr	Grashof Number (-)
I	electrical current (A)
n	PV-cell ideal factor (-)

N	number of the PV-cell in PV-panel (-)
Nu	Nusselt number (-)
N_e	clear sky factor [8 for clear; 0 for totally covered]
k	Boltzmann's constant (1.38×10^{-23} J/K)
k	thermal conductivity (W/(m·K))
K_i	PV-cell's short-circuit current temperature coefficient (A/K)
Pr	Prandtl number (-)
q	electron charge (1.6×10^{-19} C)
R	resistance (Ω)
Ra	Rayleigh number (-)
T	temperature (K)
V	voltage (V)
Greek letters	
α	absorptivity (-)
β	thermal expansion coefficient (K^{-1})
δ	thickness (m)
ε	emissivity (-)
μ	dynamic viscosity (Pa·s)
ν	kinematic viscosity (m/s^2)
ρ	density (kg/m^3)

σ Stefan Boltzmann constant (5.670367×10^{-8} W/($m^2\cdot K^4$))

τ transmissivity (-)

Subscripts

ab absorber

conv convection

con_T constant of linear variation on temperature difference

con_G constant of linear variation on irradiance difference

D diode (current)

eq equilibrium

g glass

gr ground

MPP maximum power point

oc open-circuit

p parallel

pv photovoltaic

PH photo (current)

ray radiation

RS reverse saturation

s series

S saturation

SC	short circuit
SH	shunt
STC	standard test condition
t	thermal
v	ambient vapour
wi	wind

1. Introduction

Solar energy is one of renewable energy sources that is highly untapped and underutilized. The amount of solar radiation incident on the roof of a typical home exceeds its energy consumption over a year, but it is a pattern completely opposite to the heat demand pattern and it has large summer-to-winter variations and significant diurnal variations. It is imperative to integrate energy storage unit in order to overcome the seasonal discrepancy between demand and supply and substantially increase the solar fraction of energy supply. Especially for medium and high latitude regions like the UK where the energy consumption for space heating and hot water use accounts for around 80% of the total domestic final energy consumption [1]. Since around 80% heating is provided by natural gas, there is a factor of approximately four variance between a winter peak gas demand and a summer demand. That indicates the enormous range potential required for seasonal solar heat energy storage [1]. On the other hand, hybrid PV/T systems incorporating two methods of energy conversion, i.e. photo-thermal and photo-electric conversion in one device, have received great attention for the improved energy utilization efficiency of solar sources for the past few years. It kills two birds in one stone as the thermal energy absorbed by the solar PV cell is transferred to the cooling fluid (air or liquid) through the integrated collector and used for heat applications such as space heating, domestic hot water, drying, etc.; consequently, it contributes to a lower PV cell working temperature for the improvement in electrical conversion efficiency [2, 3].

The hybrid PV/T has undergone rapid developments in recent decades. To maximise the conversion and utilisation of solar energy, many research works have primarily targeted thermal energy production and applications, as the PV panel could extract maximum of 25% of photon energy from a solar spectrum of AM1.5G while the remaining 75% is thermal energy [3]. Apart from the most influential external factors to energy conversion efficiencies such as geographical location and climate (including solar irradiance, ambient temperature, wind speed, etc.), the R&D efforts on the thermal production of hybrid PV/T systems have been mainly on the factors including the cooling fluid type, the design configuration and parameters of thermal collectors, in addition to operating parameters such as fluid flow rate and the type of application used, as the former two factors are the most important elements discussed in majority of research works. Commonly used coolants are air [4, 5] and water [4, 6-8], or a mix of the two [9, 10]. Since water has high specific heat capacity and density compared with air, the water-based hybrid PV/Ts achieve higher thermal and electrical efficiency than air-based ones [4, 5, 11]; moreover, the use of water as working fluid is more suitable for heating applications like space heating, especially domestic hot water use, or as efficient heat carry and transfer media for other downstream applications. In recent decade, there is a strong motivation to use different nanofluids (a mixture of base fluid like water or ethylene glycol, and nanoparticles) to improve the heat transfer performance and hence both electric and thermal efficiencies of the hybrid PV/T system, as nanofluids have intensified thermophysical properties, such as thermal conductivity, viscosity, and convective heat transfer coefficients compared with conventional fluids [12-15]. The drawbacks of using nanofluids are associated with high cost of nanoparticles, limited time of stability, and pressure drop in the collector. Apart from the efforts on nanofluids, incorporating PCM within the PV/T system as a heat sink is another prevailing research topic for efficiency improvement of the PV/T system in recent decade. Works proposed to add a PCM layer beneath the absorber [16], or employ microencapsulated PCM slurry [17], or embed PCM in the hot water tank [18], etc. Depending on the melting temperature of the PCM, although it has limited effect on reducing the PV cell temperature with limited cooling rate compared to water cooling system, it can effectively stabilise the transferred heat and prolong the duration of the stablised heat delivery with its high latent heat storage capacity, which could significantly improve the electric output and mitigate the thermal fatigue by limiting the peak temperature of the PV cell when the solar irradiance is the richest. Many PV/T systems with PCM also worked with addition of air or water or nanofluid cooling to further improve the thermal energy recovery [19, 20].

The collectors may have a typical sheet-and-tube (flat plate parallel tubes type, or serpentine tube type, etc.) configuration [6, 21], flat-box-type [6, 22, 23], or heat pipe [24-26], etc. The design of unglazed or glazed (with different numbers of glazing covers) [6, 13, 27, 28] and different packing factor [26, 28-30] have significant overall effect. The box-structure collector, may be built from extruded aluminum alley or made of polycarbonate material, has been reported to provide higher heat transfer and achieve higher final water-temperature and higher energy efficiency even in the thermosyphon design than the sheet-and-tube collectors [6, 31, 32]; however, the latter one is the most common and a highly appropriate option for domestic application of water-based PV/T due to high efficiency (marginally lower than that of the flat-box design [6]), easiest and most affordable configuration to manufacture as it relies on well-known, readily available technology [6, 21, 30]. The heat pipe combined PV/T design is one of effective solutions to ensure the uniform temperature of PV panel without the need of water pump, and to avoid freezing in cold regions. It has been studied for application of building integrated PV/T system (BIPV/T) [33], or integrated within the building envelop (BIPV) [34], but with modest electric efficiency (less than 10%) in most cases [2]. The glazed type PV/T is the better choice than the unglazed one if the target is to acquire more thermal output and higher overall energy efficiency, but the addition of glass covers results in higher optical losses, leading to electric efficiency decrease [4, 6, 27, 28]. The packing factor is an important parameter in PV/T system design, and the effect of its variation on the PV/T performance strongly depends on different PV/T configuration with different coolant types. Many works concluded that higher packing factors were desirable in order to maximize electrical output, but not a favorable factor for the thermal production; nevertheless, in the work [26], increasing packing factor caused higher PV panel temperature, leading to higher thermal efficiency but reversely the decreased electric efficiency; in the air-cooled collector system with double glass layer design reported in [35], the electric efficiency decreased with the increase of the packing factor, both the annual gain of electric output and thermal output was decreased. The double glass layer design significantly contributed to the higher PV panel temperature and considerable optical loss compared to unglazed or single glass cover, however, the increment of thermal production due to the higher PV module temperature may not offset the reduced heat gain attributed to the lower packing factor within the double glass cover design. Additionally, panels connection in series favors in thermal energy efficiency, whereas it reduces when panels are connected in parallel [36].

The hybrid PV/T has undergone rapid development, and there is still research gaps and the remaining questions or unexplored areas to be addressed further. For example, (1) majority of works on flat-plate water-based PV/T focused on low temperature application (<60 °C), such as space heating (air heating or radiant floor heating, <40 °C) and domestic hot water use (40~60 °C) in the context of warm or hot regions with the ambient temperatures in the range of 30~37 °C, which could be problematic yet rarely explored for cold regions with lower solar irradiance and lower ambient temperature. (2) Even for hot climate, there is scarce information on medium temperature application (>60 °C). Considering to harness the recovered heat for downstream applications, the quality and quantity of thermal production are both important to meet the operating requirement of the downstream applications. (3) Moreover, most works dealt with thermal efficiency and the improved electric efficiency during the daylight only, the benefit of storing thermal energy transferred from the PV/T system for various applications after sunset has hardly been explored [2].

Dubey and Tiwari [37] numerically studied the energy yield by 2~10 flat-plate water-based PV/T collectors (the packing factor 0.0825) connected in series under the Indian weather conditions. When the solar intensity was 600~850 W/m^2 and the ambient temperature 30~37 °C, 10 series-connected collectors produced hot water at outlet temperature max. 85 °C at a constant flow rate 0.04kg/s with the electrical efficiency of 8.7%~10.5%. In the case of coupling with a water storage tank (200 L) and the flow rate was fixed at 0.01 kg/s, the maximum temperature was achieved around 95 °C. Ibrahim et al. [38] studied a PV panel combined with rectangular-tube spiral flow absorber to produce hot water in a storage tank up to 50 °C in the Malaysian tropical climate (ambient temperature around 35 °C). Because of the increasing temperature of inlet water in a closed water loop, thermal and electrical efficiencies were decreasing throughout the day and the average values were 48% and 10.8%, respectively. Rosa-Clot et al. [39] experimented a PV/T collector called TESPI, in which a thin layer of water flowing in a polycarbonate box that was simply put on the top of the PV panel. When three collectors were series-connected, the outlet water temperature reached up to 60 °C in an open loop in some September days as the ambient temperature at around 30 °C. The total loss of electric power comparing the PV/T collector with the reference PV panel was on average 10.7%. Herrando et al. assessed the suitability of a single-cover sheet-and-tube PV/T system [30] and a polymeric flat-box PV/T system [23] for the provision of electricity and hot water for a typical house in London (low solar irradiance and low ambient temperature). The packing factor of the solar collector and the collector flow rate were specifically considered to estimate the performance of the PV/T system, and it was concluded that the coolant flow rate did not strongly influence the electrical output but affected the hot water output, while the packing factor affected the electrical output considerably more than it did the thermal equivalent. It is worth noting that although using higher coolant flow rate increases thermal efficiency, the outlet temperature of the coolant is lower, therefore requiring a greater use of auxiliary heater to further heat it to 60 °C for the domestic hot water use. Since it is not possible to maximise both outputs at the same time, a trade-off is needed depending on the end-user needs. It was suggested high packing factor (0.8~1) and low coolant flow rate as being appropriate in terms of adequately covering both the electrical and thermal demands. The results shown that a 15 m^2 sheet-and-tube PV/T system studied with a completely covered collector and a flow rate of 20L/h, can cover 51% of the total electricity demand and 36% of the total hot water demand over a year [30]; 11 flat-box PVT collectors together with a 0.83 m^3 storage tank and a constant flow-rate of 30 L/h can cover 66% of the electrical and 29% of the thermal energy demands annually [23]. Hazami et al. [40] studied the monthly and annually performance of the SCS (Solar CombiSystem with water storage tank) with a unit module area of 1.42 m^2 for the space heating load (floor heating at around 24 °C) and domestic hot water supply (at 60 °C) and the electric energy production for a 120 m^2 building occupied by 4-5 occupants. There was a shortage of thermal energy production in cold months from November to March, during which the SCS provided from 40 to 70% of the total domestic hot water needs, whereas the SCS provided about 150% of the total energy needs in hot months. Such a system allows the preservation of about 48% of electric energy supplied by the national grid, or permits the saving of about 46% of gas/gas town consumed by a gas boiler of water heating. To further achieve a net/near zero energy status for existing houses, a seasonal storage system was suggested the most appropriate solution to store the excess of energy. García et al. [41] studied the possibility of combining a heat pump supported PV/T system with a low temperature district heating network in three different configurations for a Central European multi-family house. PV/T systems provides one more solution towards low carbon and eventually zero carbon buildings, for example, the PV/T system in the hybrid configuration studied produced 34% of the heat and 55% of the electricity demand of the building, which reduced its carbon footprint by roughly 50%. In terms of energy efficiency and profitability, the key was to effectively manage the excessive heat production of the PV/T system that cannot be exploited in the building, either through reliable seasonable thermal energy storage with minimum energy loss or feeding into the district heating network. The accessibility to a low temperature district network is currently still very low everywhere and requires larger scale of retrofitting effort than constructing a stand-alone thermal energy storage system.

To maximise the utilisation of solar energy and minimise the interaction of PV/T systems with national grid, especially exporting electricity which strongly relies on the grid accommodation capacity, the varying regulation and government incentives, and with the district heating network (as foregoing), the scalable and efficient seasonable thermal energy storage system is one of the most promising solutions to be integrated with the PV/T systems, which has been for the first time explored in this work. The seasonal solar energy storage system conceived in this work innovatively integrated with the PV/T collector is the most promising long-term storage method due to its zero-loss and much higher thermal energy density than the hot water tank in the above mentioned studies and latent heat storage. More comprehensive knowledge and information about thermochemical sorption technology and the comparison between different seasonal storage technologies can be found in review articles [42-48]. Ma et al. [49] explored the feasibility of applying different technologies of seasonal solar thermal energy storage in domestic dwelling in the UK, and estimated the volume of a sorption storage system to satisfy 100% solar fraction was 31.5~44.3 m^3 for different UK cities studied, in contrast with the water storage system that required a volume of 107~150 m^3. However, such an integration requires relatively demanding operational condition, energy charging process through the endothermic desorption happens at comparatively higher temperature than the hot water use reported in the above studies, for example, the typical working pair $SrCl_2$/ammonia has the equilibrium desorption temperature at around 95 °C, respectively when heat sink temperature at 30 °C. The closed water loop cannot be considered in this situation, because the return water from thermochemical system still has relatively high temperature, which is detrimental for both electrical and thermal efficiency. Therefore, with an open loop water heating, this work investigated the energy output and efficiencies of a PV/T collector that produces relatively high temperature hot water to be used for thermochemical sorption cycles. The most common and mature design of the PV/T collector, a completely PV panel-covered sheet-and-tube PV/T collector with single glass cover and an air insulation layer between the glass cover and the PV panel, was considered as a highly suitable starting point towards the target of thermal production as priority at a reasonable cost. Unlike the above studies using fixed flow rate of the heat removal fluid, water flow rate was adjusted in the current work depending on the variable solar irradiation to achieve the required temperature threshold for the thermochemical process. Using a CFD model coupled with a detailed PV panel model and the real weather data of the city of Newcastle upon Tyne in the UK, dynamic performance of the PV/T collector was numerically and parametrically investigated to explore the potential of such a novel integrated system for seasonal solar storage application in the England climate. The influence of the varying water flow rate and the high temperature of water output on the efficiencies of the PV/T collector was also analyzed and discussed.

2. Working principles

2.1. PV/T solar collector

Solar radiation that reaches the PV layer is absorbed in two forms, electricity and heat. A portion of visible light waves was absorbed to produce electrical current; infrared and the rest of visible light waves are mostly absorbed in the form of heat and transferred to neighbouring layers: conductive heat transfer to the absorber eventually extracted by the heat transfer fluid (HTF) flowing through the tubes, natural convective heat transfer to the air gap layer and radiative heat transfer to the glass cover layer. Further radiative heat transfers from the glass cover layer to sky and ground is also considered in some studies pursuing highly accurate results [50]. The impact of the glass encapsulation and the adhesive layer on the heat transfer can be neglected due to their very thin thickness, negligible thermal mass and good heat transfer properties.

Figure 1~~Figure 1~~ shows a typical sheet-and-tube photovoltaic-thermal collector studied in this work, which consists of a single glass cover, PV-cells, tubes, HTF (inside the tubes), and insulation. Many developed configuration of flat plate PV/T collectors differ from each other, like unglazed or glass-covered PV cell with or without an air gap between the glass cover and the PV cell, coupled with an air-based, or water-based or bio-fluid thermal collector. Unglazed design is more favourable if the electrical power generation is of priority, which allows quick heat dissipation of the PV cell through natural convection, leading to improved electrical conversion but compromised thermal efficiency. On the contrary, a glass cover generates optical loss and prevent natural ventilation, resulting in the reduction of PV cell performance, whereas, the glass cover strongly increase the thermal performance of the thermal collector, leading to a better overall thermal energy conversion [51]. An air gap acts as a thermal insulator to prevent the conduction heat transfer between the PV cell and glass cover layers, it is normally used to minimize the heat loss and further enhance the thermal performance especially targeting comparatively higher output temperature. Water-based collector is studied in this work due to its greater heat transfer properties [52] compared to air-based system, and a water tank is used to collect and store the thermal output from the PV/T collector for other applications that require relatively higher temperature heat, such as domestic hot water use (>50 °C) or thermochemical storage (>70 °C), as shown in Figure 2~~Figure 2~~of the system schematic.

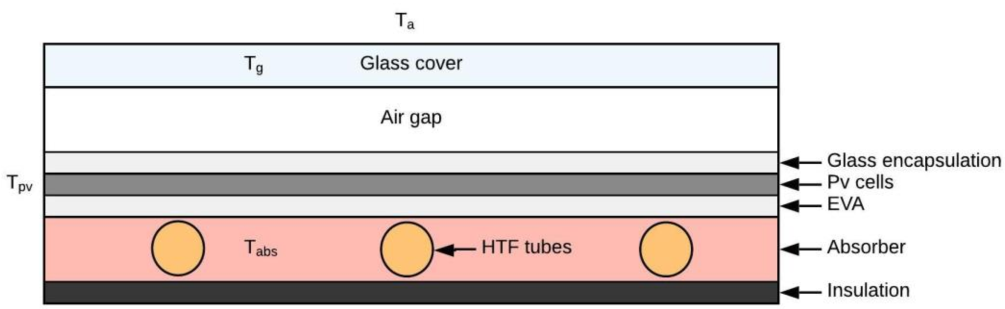

Figure 1. A typical flat plate glass-covered water PV/T collector

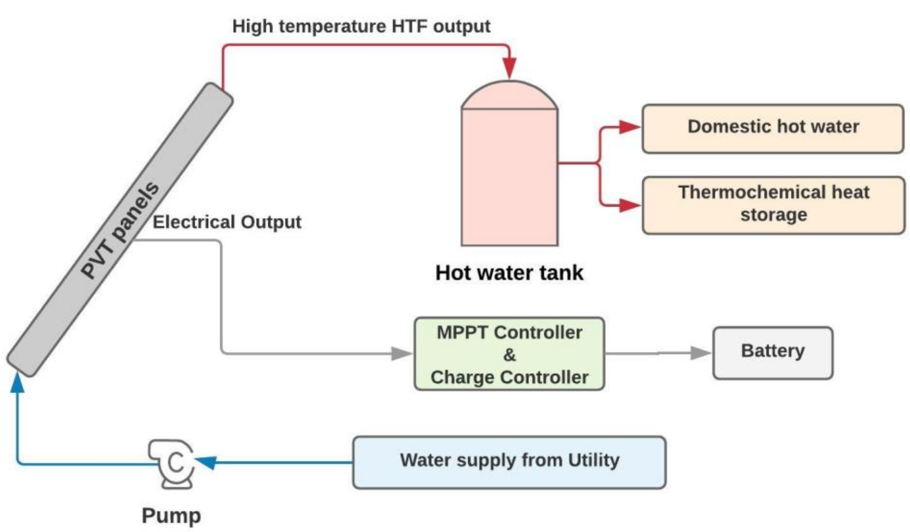

Figure 2. System schematic

2.2. Thermochemical sorption storage

A basic thermochemical sorption system comprises two vessels, one contains adsorbent material, the other one is filled with liquid/vapour refrigerant as the condenser/evaporator as shown in Figure 3~~Figure 3~~. The thermochemical sorption cycle uses the reversible reaction between adsorbents like halide salt ammines and the refrigerant like ammonia to realise the energy charging and discharging process. During the charging process, the salt ammine adsorbent is heated to desorb refrigerant vapour which gets cooled down and condenses in the condenser, thus the thermal energy is stored in the form of chemical potential without energy loss for long term storage. In the discharging phase, the liquid refrigerant extracts heat from the available heat source (i.e. ambient air, river or lake or ground water) and evaporates, while the salt ammine adsorbent adsorbs the refrigerant vapour and releases considerable amount of adsorption heat for heating purpose.

$$SrCl_2 \cdot NH_3 + 7NH_3 \leftrightarrow SrCl_2 \cdot 8NH_3 + \Delta H \quad (1)$$

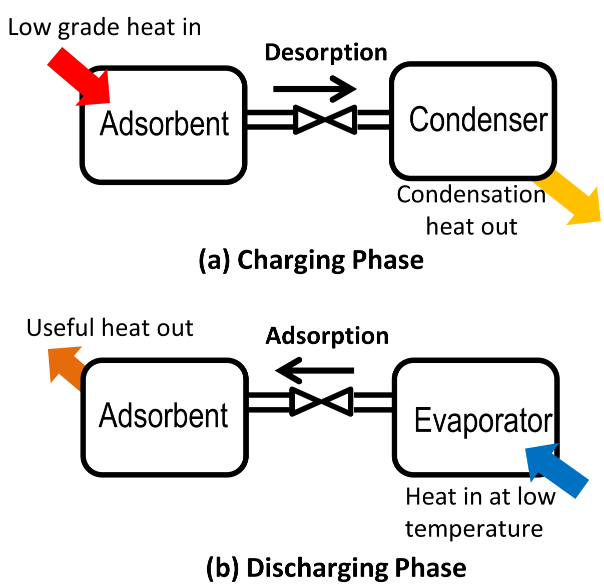

Figure 3. A basic thermochemical sorption cycle for energy storage.

The typical working pair of $SrCl_2$-NH_3 was applied in this work to be integrated with the PV/T-AG collector for solar thermal seasonal storage. The chemical reaction between the $SrCl_2$ ammine and ammonia is expressed in Eq. (1)~~(1)~~, and the studied cycle depicted in the P-T diagram is shown in Figure 4~~Figure 4~~. The hot water output from the PV/T-AG collector was used for desorption process in the charging phase. For example, when the average condensation temperature is around 15 °C by air-cool method, the required desorption temperature should be at least around 90 °C with an equilibrium temperature drop of 5 °C. The equilibrium drop is defined as the difference between the equilibrium condition and its actual state, which is the main driving force of the chemical reaction [53]. That suggests the PV/T-AG collector should produce hot water at around 100 °C if there exists a heat transfer difference of 10 °C. It should be noted that after the hot water supplies heat to the thermochemical sorption system it goes to the water tank as its temperature is still sufficiently high for domestic hot water use. In the discharging phase, the system runs as a water source heat pump, refrigerant evaporator extracts heat from the water source that has more stable and higher temperature (typically 10 °C in the winter) than the ambient air, in the meantime, the adsorption heat is required at least 70 °C to provide proper domestic hot water (at around 60 °C), with a heat transfer temperature difference of around 10 °C.

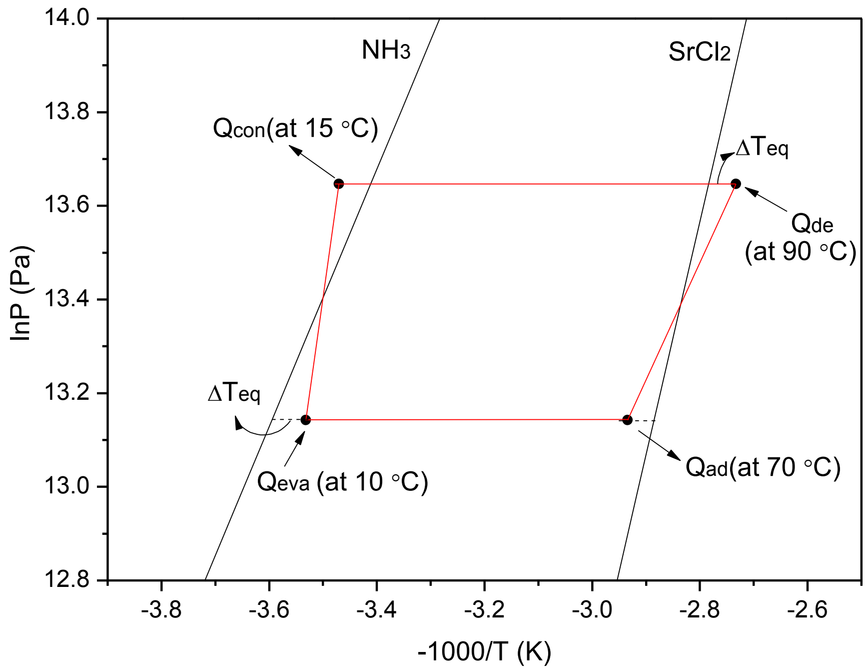

Figure 4. The thermochemical sorption cycle using working pair $SrCl_2$-NH_3 in the P-T diagram.

3. Modelling and simulation

The overall performance of the PV/T system including electricity and thermal output depends on the solar energy input, the ambient temperature, wind speed, the operating temperature of the system parts and the heat extraction conditions such as the inlet and outlet temperature and the mass flow rate of the HTF. Two different designs of the single glass-covered sheet-and-tube PV/T collectors, with and without airgap, have been analysed and compared with the reference PV module to reveal more insights. PV/T collectors without airgap are already available off-the-shelf, and measurement data is easily available for model validations in this work. The weather data in 30-minute time step from sunrise to sunset of Newcastle-upon-Tyne, a representative high-latitude city in the UK, including atmospheric temperature, global horizontal radiation and wind speed, is available from the software Meteonorm.

Unlike majority of the reported systems coupled with a water tank, which used a closed loop as the inlet water temperature of the PV/T collector was gradually increasing throughout the process since the water temperature in the tank was increasing, in this work it was an open loop of water circulation with a fixed inlet temperature (i.e. at the ambient temperature) and a certain temperature threshold of the outlet water in order to meet the requirement of the downstream application (e.g. 60 °C for hot water use, >70 °C for thermochemical storage). In this instance, according to the varying weather conditions, the mass flow rate of the water should be adjusted to ensure the required outlet water temperature, instead of a fixed value of the HTF flow rate. Therefore, it is important to study the influence of such operating conditions on the individual electrical and thermal efficiency and the overall energy conversion efficiency of the PV/T collector and gain insights of the potential of the PV/T collector integrated with thermochemical sorption system.

The temperature variation profile of the system components was simulated and analyzed in ANSYS Fluent coupled with a detailed model of the PV cell developed in the Matlab. The methodology to simulate the simultaneous generation of electrical power and thermal power from the PV/T collector is illustrated in Figure 5~~Figure 5~~. A one-diode current-voltage (I-V) model was developed using Matlab Simulink to represent the relationship between the electrical generation performance of the PV cell and the varying solar irradiance and cell temperature when the load voltage varies from 0 to open circuit voltages. The measured data of Siemens SM46 PV module and Solarex MSX60 PV module presents the current-voltage characteristics under the standard test condition (STC, i.e. the PV cell temperature at 25 °C and the irradiance of 1,000 W/m^2) was used to validated the PV cell model. To assure the generic application of the I-V model developed in this work it was also verified against the measured data of the Solarex MSX-60 PV module at the irradiance of 1,000 W/m^2 and temperature ranges from 0 to 75 ^{o}C in addition to the STC. Since there is little information reported for a full set of experimental data on the PV/T collectors, the thermal analysis model were also validated using the measured PV cell temperature of the same commercial PV modules.

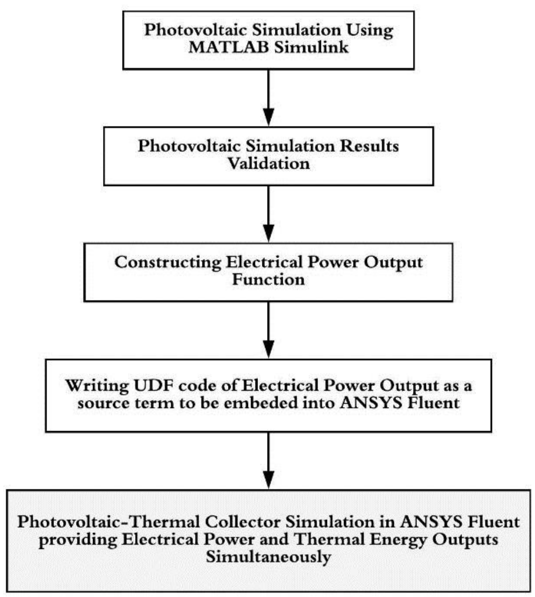

Figure 5. The methodology of simultaneous simulation of electrical and thermal energy in the photovoltaic containing panels.

3.1. PV cell model development and validation

Instead of the simplified expression of electrical efficiency reported in Ref.[54] which was extensively used for the PV/T research works [55], the one-diode model [56] (Figure 4) was used to simulate the electrical production of the PV cell with significantly improved accuracy of dynamic performance. Kirchhoff's current law is used at the circuit node of the photocurrent output (I_{PH}) in Figure 6~~Figure 6~~ (a) and (b), which states that the summation of currents at any circuit nodes is zero.

A PV panel consists of a number of the PV cell connected in series (N_S cells) and parallel (N_p lines) as represented by the diodes in Figure 6~~Figure 6~~ (a). In majority of the previous research works, the ideal conditions was assumed as shown in Figure 6~~Figure 6~~ (a) as all PV cells were perfectly manufactured and there was no internal resistance through the wiring between the PV cells. However, for a more accurate model, the wiring resistance between PV cells and the recombination loss between the P-N junctions of PV cells should be taken into account, which are represented as R_S and R_{SH}, respectively, in Figure 6~~Figure 6~~ (b), where the I_D represents the combined diode currents of those shown in Figure 6(a). The current (I) that passes through R_S and goes to the load can be expressed in Eq. (2)~~(2)~~ which is the output current of the PV panel. I_{PH} is the photo current generated from the doped semiconductor used in the PV cells, and it varies depending on the PV cell temperature and the solar irradiance and can be calculated from Eq. (3)~~(3)~~. The I_D in Figure 6~~Figure 6~~ (b) is calculated from Eq. (4)~~(4)~~. I_{SH} is the shunt current obtained from Eq. (5)~~(5)~~. The elements in Eqs. (3)~~(3)~~ - (5)~~(5)~~ to calculate currents are the characteristics of the PV cell material, where I_{SC} are the short-circuit current of the PV cell provided by the manufacturer while the saturation current (I_S) and the reverse saturation current (I_{RS}) of the PV cell can be calculated by Eqs. (6)~~(6)~~ and (7)~~(7)~~, respectively [57].

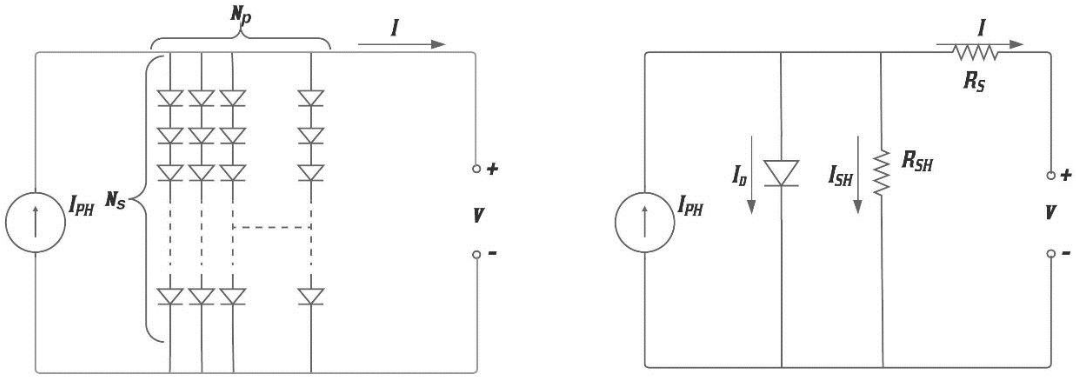

(a) (b)

Figure 6. (a) PV cell model using diodes model connected in series and parallel; (b) Photovoltaic based on the one-diode model.

$$I = I_{PH} - I_D - I_{SH} \tag{2}$$

$$I_{PH} = N_p[I_{SC} + K_i(T_{pv} - T_{pv\_STC})]\frac{G}{G_{STC}} \tag{3}$$

$$I_D = N_p I_s\left\{exp\left(\frac{q}{kT_{pv}n}\left(\frac{V}{N_s} + \frac{IR_s}{N_p}\right)\right) - 1\right\} \tag{4}$$

$$I_{SH} = \frac{N_p V + N_S I_{RS}}{N_S R_{SH}} \tag{5}$$

$$I_S = I_{RS}\left(\frac{T_{pv}}{T_{pv\_STC}}\right)^3 \times exp\left(\frac{qE_g}{kn}\left(\frac{1}{T_{pv\_STC}} + \frac{1}{T_{pv}}\right)\right) \tag{6}$$

$$I_{RS} = \frac{I_{SC}}{exp\left(\frac{V_{oc}}{N_s n V_t}\right) - 1} \tag{7}$$

The characteristics and the behavior of the PV cell (Siemens SM46 PV module and Solarex MSX-60 PV module) at the STC summarized in Table 1~~Table 1~~ was used to solve Eqs. (2)~~(2)~~ to (7)~~(7)~~. The series resistance (R_S) and the shunt resistance (R_{SH}) are the causes of power loss from the PV cell which alters the slope of the I-V curve and reduces the maximum power. According to Carrero, et al. [57], the R_S and R_{SH} could be estimated corresponding with the value of V_{OC}/I_{SC}, but those values should be different for different PV cells; moreover, the R_S and R_{SH}

should not be constant values under different conditions of irradiation and cell temperaure. In this work, the initial values of R_{SH} and R_S were defined as 54 Ω and 0.54 Ω suggested by Carrero, et al. [57] for Eqs. (8)~~(8)~~ and (9)~~(9)~~ respectively to start the iterative calculation; the Euclidean or the norm error (L^2) (Eq. (10)~~(10)~~) was being monitored during the iteration, as this error reduced as the iteration proceeds. Therefore, the values of the R_S and R_{SH} were adjusted along the iteration until the L^2 norm error stopped reducing, which was 0.1671 for Siemens SM46 PV model in this study.

$$R_{S\_STC} < 0.1\frac{V_{oc}}{I_{SC}} \tag{8}$$

$$R_{SH\_STC} > 10\frac{V_{oc}}{I_{SC}} \tag{9}$$

$$L^2 \text{ norm error} = \sqrt{\sum_{i=1}^{n}(u_e(i) - u_c(i))^2} \tag{10}$$

where the L^2 norm error represents the overall error of a dataset from a multi-point measurement, u_e(i) and u_c(i) is the measured value and the calculated value at point i, respectively, and n is the number of data points.

Based on the comparison between the simulated I-V and P-V curves and the measured data, the values of the series resistance (R_S) and the shunt resistance (R_{SH}) under different conditions of irradiation and cell temperature were obtained through iterative calculation. Hence, the new correlations of the R_{SH} as a function of the R_{SH_STC} and the ratio of the actual irradiation and the STC irradiation was developed and verified in this work as presented in Eq. (11)~~(11)~~. The R_S as a function of the R_{S_STC}, the cell temperature difference and the irradiation difference between the actual value and the reference value was proposed and verified as Eq. (12)~~(12)~~.

$$R_{SH} = R_{SH\_STC}\frac{G}{G_{STC}} \tag{11}$$

$$R_S = R_{S\_STC} + R_{S_{con_T}}\left(T_{pv} - T_{pv_{STC}}\right) - R_{S_{con_G}}(G - G_{STC}) \tag{12}$$

where T_{pv_STC} is 25 °C, $R_{S\_con\_G}$ is the constant for the irradiance dependent term, G_{STC} is 1,000 W/m^2.

The electrical power output of the PV cell can be obtained by multiplying its output current (I) with the connected load's voltage (V). If the connected load voltage is constant such as a 12V lead acid battery, the connected load voltage may not be at the maximum power point that the PV cell can provide at that specific irradiance due to the variation and intermittence of the solar irradiation. Practically, a maximum power point controller is installed between the PV panels and loads to increase or decrease the loads voltage meanwhile the output current changes with the varying load voltage according to its I-V characteristics, irradiance and cell's temperature, in order to extract the maximum power from the PV panel at every incoming irradiance and cells' temperature. Therefore, the maximum power output (P_{max}) was considered as the electrical power output of the PV layer (E_8) in this study and can be calculated from Eq. (13)~~(13)~~.

$$P_{max} = E_8 = V_{P\_max} \cdot I_{P\_max} \tag{13}$$

where V_{p_max} is the load's voltage at maximum power point; I_{p_max} is the output current at maximum power point. After model validation, the PV power output is simulated using the validated model espressing I-V characteristics of the PV cells for the condition of the irradiance ranging from 0 to 1,000 W/m^2 and the PV cell temperature between 0 ^{o}C and 100 ^{o}C. The simulated data of the electrical power output was then fitted for the polynominal regression of the relationship between the electrical power output and the weather conditions. In this paper, the simulation was conducted in 30 minutes time-step as the electrical efficiency at each time-step may vary. The electrical efficiency (η_{elec}) was calculated from Eq. (14)~~(14)~~. If the average daily efficiency was considered, the integration interval (from t_1 to t_2) was from sunrise to sunset and if the instantaneous thermal efficiency was considered, the integration interval was 30-minute.

$$\eta_{elec} = \frac{\int_{t_1}^{t_2} E_8 \, dt}{\int_{t_1}^{t_2} Irr \, dt} \tag{14}$$

where Irr is the solar irradiance as a function of time of the day (W/m^2).

Table 1. Characteristics of the PV cells at STC.

Characteristics of the PV module	Siemen SM 46	Solarex MSX-60
Typical peak power (P_{MPP})	46 W	60 W
Voltage at peak power (V_{MPP})	14.6 V	17.1 V
Current at peak power (I_{MPP})	3.15 A	3.5 A
Short-circuit current (I_{sc})	3.35 A	3.8 A
Open-circuit voltage (V_{oc})	18.0 V	21.1 V

Characteristics of the PV module	Siemen SM 46	Solarex MSX-60
Temperature coefficient of open-circuit voltage (K_v)	-77 mV/°C	-80±10 mV/°C
Temperature coefficient of short-circuit current (K_i)	12 mA/°C	0.065±0.05 %/°C
the ideal factor of PV cell	1.2	1.2
Band-gap energy of semiconductor	1.16 eV	1.16 eV
Number of PV cells in series	30	36
Number of PV cells in parallel	1	1

3.2. Thermal analysis models

Two types of the PV/T collectors were studied and compared with a reference PV module in this paper, which are the PV/T collector without air gap (PV/T-no-AG) and the PV/T collector with air gap (PV/T-AG). The cross-sectional view of these two designs modelled in ANSYS Fluent is presented in Figure 7~~Figure 7~~ (a) and (b) respectively. The air gap between the glass cover and the PV panel in Figure 7 (b) acts as an air insulation layer, which is favourable for thermal production. The reference PV module was modelled almost the same as the PV/T-no-AG model but without the absorber beneath the PV cell. The dimensions of all models are presented in Table 2.

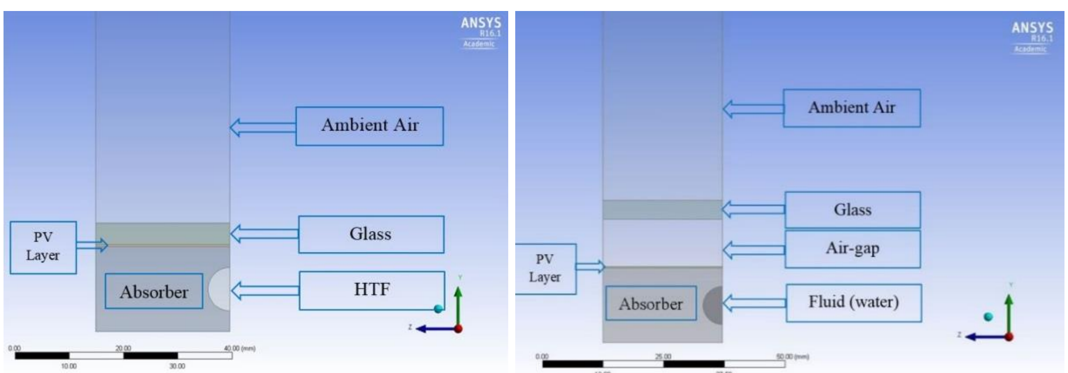

(a) (b)

Figure 7. Cross-sectional view of the PV/T collector (a) without an air gap (b) with an air gap in ANSYS Design Modellor.

Table 2. Dimension data of the PV and PV/T collectors studied.

	PV-panel model	PV/T-no-AG model	PV/T-AG model
Ambient air thickness or Upper air thickness (Y-axis)	300 mm	300 mm	300 mm
Lower ambient air thickness (Y-axis)	300 mm	300 mm	300 mm
Glass thickness (Y-axis)	-	4 mm	4 mm
Air-gap thickness (Y-axis)	-	-	10 mm
PV layer thickness (Y-axis)	0.3 mm	0.3 mm	0.3 mm
Absorber thickness (Y-axis)	15.7 mm	15.7 mm	15.7 mm
Fluid tubes' diameter	-	8 mm	8 mm
All components' length (X-axis)	1830 mm	1830 mm	1830 mm
Cut models' width (Z-axis)	24.65 mm symmetry	24.65 mm symmetry	24.65 mm symmetry
Full model width (Z-axis)	986 mm	986 mm	986 mm
Length between 2 fluid tubes	-	49.3 mm	49.3 mm

The energy balance is dominated by heat conduction in the solid elements including glass cover, PV cells and absorber (including tubes), as expressed in Eq. (15)~~(15)~~.

$$\rho_m \delta_m C_m \frac{dT_m}{dt} = k_m \delta_m \left(\frac{\partial^2 T_m(x,y,z)}{\partial x^2} + \frac{\partial^2 T_m(x,y,z)}{\partial y^2} + \frac{\partial^2 T_m(x,y,z)}{\partial z^2} \right) + \sum Q_m \qquad (15)$$

where the subscriber 'm' is replaced by different symbols to represent different elements, e.g. 'g' when the glass layer is under consideration, or 'pv' when the PV-layer is discussed, or 'ab' for the case of the absorber layer; ΣQ is the summation of different heat sources for each layer. For all different models studied, the energy balance of the single glass cover (ΣQ_g) for example expressed in Eq. (16~~(16~~) includes the solar radiation to the glass cover Q_1 (Eq. (17)~~(17)~~), the sky radiation to the glass cover Q_2 (Eq. (18)~~(18)~~), the convective heat from ambient air to the glass Q_3 (Eq. (19)~~(19)~~), the radiative heat from the glass to PV cell Q_4 (Eq. (20)~~(20)~~, and the radiative heat from the glass to ground Q_5 (Eq. (21)(21)). For the PV/T-AG model, the convective heat between the glass and the PV cell according to natural convection in the air layer Q_{6_a} was calculated in (Eq. (22)(22)) and replace the Q_6 in Eq.(16)(16); whereas, for the PV/T-no-AG and the PV panel models, the conductive heat transfer between the glass and PV surface Q_{6_b} (Eq. (23)(23)) was used to replace the Q_6 in Eq. (14)(14). Note that the positive signs in Eq. (16(16) mean the heat is absorbed by the layer envisaged and minus signs represent the heat released from the layer envisaged.

$$\sum Q_g = Q_1 + Q_2 + Q_3 - Q_4 - Q_5 - Q_6 \tag{16}$$

$$Q_1 = \alpha_g G \tag{17}$$

$$Q_2 = \varepsilon_g \sigma ({T_{sky}}^4 - {T_g}^4) \tag{18}$$

$$Q_3 = h_{wi}(T_a - T_g) \tag{19}$$

$$Q_4 = h_{ray,g\rightarrow pv}(T_g - T_{pv});\ h_{ray,g\rightarrow pv} = \frac{\sigma(T_g^2+T_{pv}^2)(T_g+T_{pv})}{\frac{1}{\varepsilon_{pv}}+\frac{1}{\varepsilon_g}-1} \tag{20}$$

$$Q_5 = \varepsilon_g \sigma ({T_g}^4 - {T_{gr}}^4) \tag{21}$$

$$Q_{6\_a} = h_{conv,g\rightarrow pv}(T_g - T_{pv}) \tag{22}$$

$$Q_{6\_b} = h_{cond,g\rightarrow pv}(T_g - T_{pv}); \tag{23}$$

Sky temperature can be approximately calculated by using Eq. (24)(24) [58] where L_0, A, B and C are obtained from Eqs. (25)(25) to (28)(28) respectively with the ambient vapour pressure (P_v) calculated by Eq. (29)(29) [59]. Ground temperature is approximately 2 °C lower than ambient temperature [60].

$$T_{sky}=\left(\frac{L_0(1+0.01A)+\frac{BC(8-N_e)}{8}}{\sigma}\right)^{0.25} \tag{24}$$

$$L_0 = 3.6(T_a - 273.15) + 231 \tag{25}$$

$$A = 10.1\ln(P_v) - 12.3 \tag{26}$$

$$B = 1.7(T_a - 273.15) + 107 \tag{27}$$

$$C = -0.22\ln(P_v) + 1.25 \tag{28}$$

$$P_v = 611.21\exp\left\{\left(18.678 - \frac{T_a}{234.5}\right)\left(\frac{T_a}{257.14+T_a}\right)\right\} \tag{29}$$

To accurately calculate Q_{6_a} in Eq. (22)~~(22)~~, natural convection theory is considered in the air-gap layer of the PV/T-AG and $h_{conv,\, g\rightarrow pv}$ is obtained from Eq. (30)~~(30)~~ where the Nusselt number (Nu_{gap}) can be calculated by Eq. (31)~~(31)~~, where θ is the tilt angles of the PV/T-AG which is valid from 0° to 75°, *Ra* is the Rayleigh number defined as the production of Grashof Number (*Gr)* and the Prandtl number (*Pr)*.

$$h_{conv,g\rightarrow pv} = \frac{Nu_{gap}k_{gap}}{\delta_{gap}} \tag{30}$$

$$Nu_{gap} = 1 + 1.44\left[1 - \frac{1708}{Ra\delta_a cos\theta}\right]\left[1 - \frac{1708(sin\theta)^{1.66}}{Ra\delta_a cos\theta}\right] + \left[\frac{(Ra\delta_a sin\theta)^{0.33}}{5830} - 1\right] \tag{31}$$

For the pv layer of all three models, the transient energy balance can be analysed using Eq.(15)~~(15)~~ with PV cell material properties and ΣQ_{pv} given in Eq. (32)~~(32)~~. Q_7 is the heat absorbed by PV layer from the solar irradiance which can be calculated by Eq.(33)~~(33)~~; E_8 is the electrical power production in the PV layer which is described in the previous section and Q_9 is the conductive heat from the PV layer to the absorber layer as presented in Eq.(34)~~(34)~~ with its thermal contact conductance coefficient $h_{cond,pv\rightarrow abs}$ calculated from Eq. (35)~~(35)~~.

$$\sum Q_{pv} = Q_4 + Q_5 + Q_7 - E_8 - Q_9 \tag{32}$$

$$Q_7 = \alpha_{pv}\tau_g G \tag{33}$$

$$Q_9 = h_{cond,pv\rightarrow abs}(T_{pv} - T_{abs}); \tag{34}$$

$$h_{cond,pv\rightarrow abs} = \frac{1}{\frac{\delta_{pv}}{k_{pv}} + \frac{\delta_{abs}}{k_{abs}}} \tag{35}$$

The energy balance in the absorber layer of the PV/T-no-AG and PV/T-AG models can be expressed as shown in Eq. (36)~~(36)~~ where Q_{10} is the convective heat transfer from the absorber layer to the HTF (Eq. (37)~~(37)~~). For the PV panel model where there is no HTF, Q_{10} represents the convective heat transfer from the absorber to the ambient air (Eq. (38)~~(38)~~). The material properties used in the models are presented in Table 3~~Table 3~~.

$$\sum Q_{abs} = Q_9 - Q_{10} \tag{36}$$

$$Q_{10\_a} = h_{abs-HTF}(T_{abs} - T_{HTF}) \tag{37}$$

$$Q_{10\_b} = h_{wi}(T_{abs} - T_a) \tag{38}$$

Table 3. The material properties used in the PV and PV/T collectors models.

Material properties	Glass	PV cell	Absorber (Aluminium)	Air	HTF (water)
Absorption coefficient, α (-)	0.05	0.8	-	-	-
Density, ρ (kg/m^2)	2,200	700	2719	1.225	998.2
Emissivity, ε (-)	0.88	-	-	-	-
Specific heat capacity, Cp (J/(kg·K))	670	900	871	1,006	4,182
Thermal conductivity, k (W/(m·K))	0.9	144	202.4	0.0242	0.6
Transmistivity, τ (-)	0.91	-	-	-	-
Viscosity, (kg/m·s)	-	-	-	1.7894e-05	0.001003

Note: Only the relevent properties of the materials used in the models are presented in the table.

In the fluid regions including the ambient air and HTF, the continuity, energy, momentum and turbulence equations were treated using the finite volume approach to computationally solve the transport equations in Eq. (39)(39) in ANSYS Fluent, where $\phi = 1$ for continuity equation, $\phi = \vec{V}$ for momentum equations, and $\phi = h$ for energy equation [61]. The first term on the left-hand side of Eq. (39)(39) is the unsteady term, the second term is the convective term, the first term on the right-hand side is the diffusion term and the last term on the right-hand side is the generation term.

$$\frac{\partial}{\partial t}\int_V \rho\emptyset dV - \oint_A \rho\emptyset\, \vec{V}\cdot d\,\boldsymbol{A} = \oint_A \Gamma_\emptyset \nabla\emptyset \cdot d\,\boldsymbol{A} + \int_V S_\emptyset dV \tag{39}$$

Turbulent flow by using SST k-omega (2 equations) model was chosen along with the viscous heating option to get more accurate solutions especially in viscous heating cases such as the heat transfer between solid and fluid zones. Low-Re Corrections was selected in the cases of low Reynolds number flow. There was a big temperature gradient along the PV/T panel from the inlet side to the outlet side, so the volume weighted average of the simulated

PV temperature was used in this work. To reduce the computational time, ground and sky was treated as source terms in the unit of W/m^3.

In this study, the useful thermal efficiency (η_{th}) was considered and it was calculated from Eq. (40)(40). Note that if the temperature of the HTF could not reach the setting temperatures, the pump would not operate and the mass flow rate would be zero, in this instance, the instantaneous thermal efficiency would be zero based on the Eq. (40)(40), even though the temperature of the HTF raised inside the PV/T. Again, if the overall average thermal efficiency was considered, the integration interval (from t_1 to t_2) was the time from sunrise to sunset; the integration interval was 30 minute for the calculation of the instantaneous thermal efficiency.

$$\eta_{th} = \frac{\int_{t_1}^{t_2} \dot{m} C_{P\_HTF} (T_{out} - T_{in}) dt}{\int_{t_1}^{t_2} \mathrm{Irr}\ \mathrm{dt}} \tag{40}$$

where $\dot{m}$ is the mass flow rate of the HTF out from 1 m^2 PV/T collectors; C_{P_HTF} is the specific heat capacity of the HTF ; T_{out} is the output temperature of the HTF from the PV/T; T_{in} is the input temperature of the HTF to the PV/T.

4. Results and discussion

4.1. Model validation

Using the developed correlations of R_{SH} and R_S in Eqs. (11)(11) and (12)(12), the calculated I-V characteristic under different conditions satisfactorily agree with the datasheets of the Siemens SM46 PV module and the Solarex MSX-60 PV module as shown in Figure 8Figure 8 and Figure 9Figure 9 respectively.

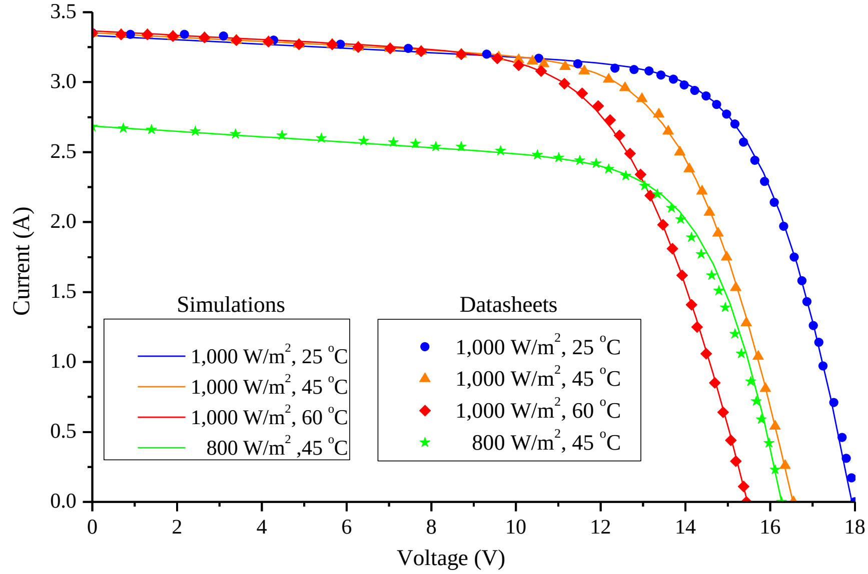

Figure 8. Verification of simulation results with datasheet of I-V characteristics in different conditions for Siemens SM46 PV module.

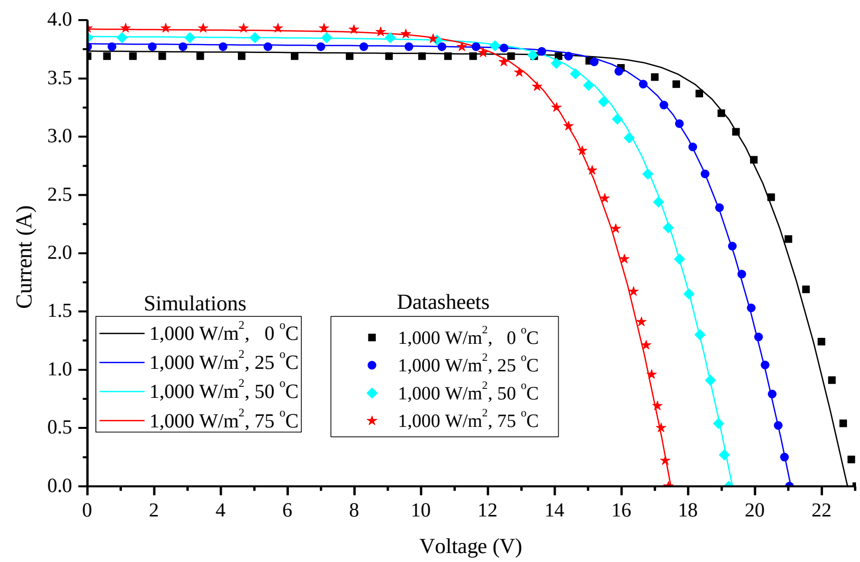

Figure 9. Verification of simulation results with datasheet of I-V characteristics in different conditions for Solarex MSX-60 PV module.

Compared to using the R_S and R_{SH} value from the calculation of V_{OC}/I_{SC}, using these modified equations of R_S and R_{SH} made the average error of electrical power output at MPP reduce from 1.59% to 0.52% for Siemens SM46 PV module, from 1.50% to 1.04% for Solarex MSX-60 PV module. The reduction of the average error over the low PV cell temperature range studied are insignificant, the errors at medium to high PV cell temperatures are substantially decreased. For example, the error of the PV power outputs operating at 60 °C at MPP reduces from

3.57% to 0.85% for Siemens SM46 PV module. Therefore, when the PV cell is used at medium to high temperatures, the modified correlations in Eqs. (11)~~(11)~~ and (12)~~(12)~~ are worth applying for better accuracy. The developed PV model that uses the modified equations of R_S and R_{SH} was also validated by using one-day real weather data and the experimental data of electrical power output from Ref. [56]. Figure 10~~Figure 10~~ shows the great agreement between the simulated PV electrical power output at MPP and the measured data reported in Ref. [56], the average error is 2.55% with 0.66 W average absolute difference. To validate the thermal analysis model, the simulation results of the PV cell temperatures was compared with the measured data provided by Ref. [56] (in Figure 11~~Figure 11~~), there was an average relative error of 4.57% with an average absolute difference of 2.03 K, that implies that the PV model coupled with the CFD model developed in this work is reasonably reliable.

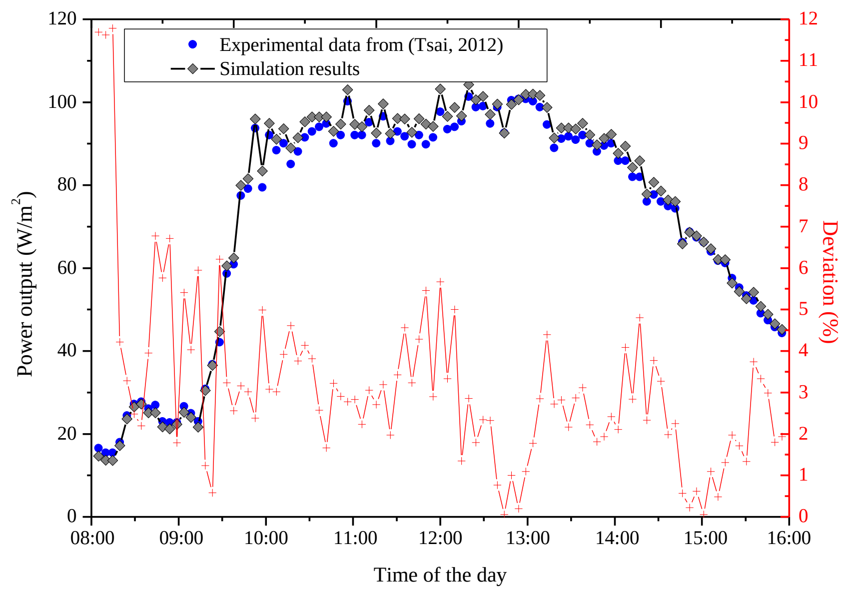

Figure 10. PV Electrical power output between the measured data from [56] of and the simulation results.

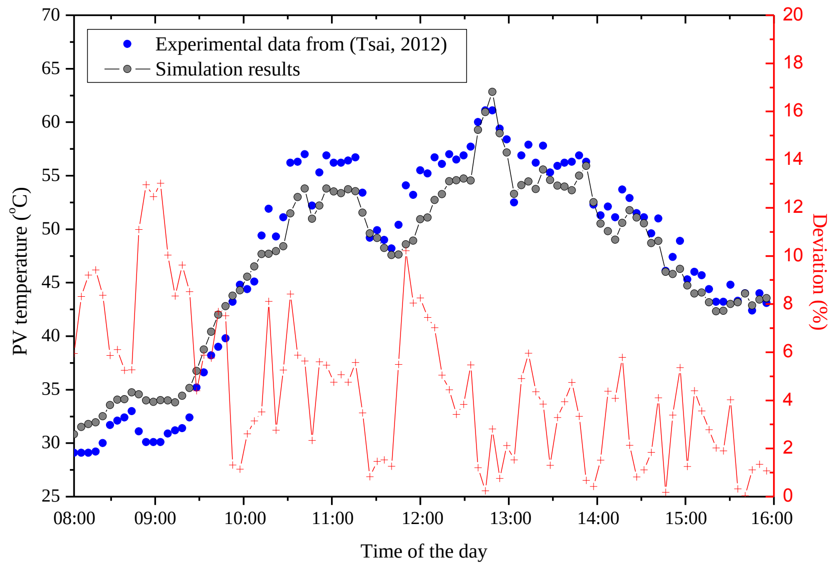

Figure 11. PV temperatures between the measured data from [56] and the simulated volume-weighted average temperature.

4.2. PV/T collector simulation results

The weather data of a sunny summer day (June 28th 2005) in Newcastle Upon Tyne are used as a case study to explore the potential hot water production by the studied PV/T collector. The water outlet temperature was preset at four targeted points, 40 °C, 60 °C, 80 °C and 100 °C, which was achieved by varying the water flow velocity so that to cope with the desorption heat requirement of the thermochemical sorption storage unit.

The half-hourly variation profile of the hot water output temperature at different preset points and the corresponding solar irradiation is shown in Figure 12~~Figure 12~~ for the PV/T with air gap (PV/T-AG). The calculation started when solar radiation was firstly available on the chosen days. The inlet water temperature was assumed to be the same temperature as the ambient temperature (around 14 °C). Solar irradiance was increasing in the morning, but it was not intense enough to heat up the water in the absorber tube to the targeted temperature levels until 07:00 ~10:00 am in summer, depending on different targets. Before that it was assumed a stagnation condition of the water loop, i.e. no fluid flowing in the collector, until the stationary water was heated up to the targeted temperature resulting in the uniform increasing temperature over the PV/T panel area. Since then, the water circulation started and the flow rate was afterwards adjusted according to the varying irradiation as shown in Figure 13~~Figure 13~~.

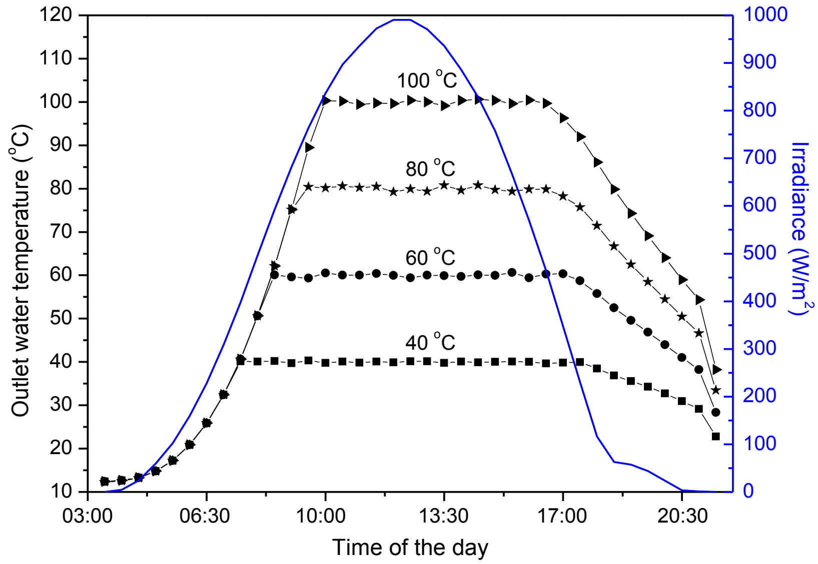

Figure 12. The water output temperature at different targeted levels from the PV/T with airgap collector on a sunny summer day in Newcastle upon Tyne, UK.

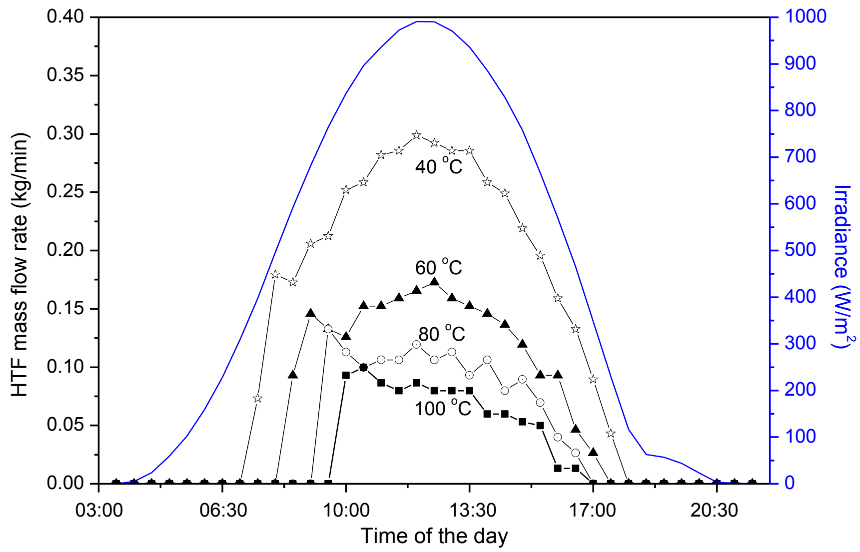

Figure 13. The mass flow rate of the output fluid at different targeted temperature from the PV/T with air gap models on a sunny summer day in Newcastle upon Tyne, UK.

The lower targeted output temperature, the higher water mass flow rate allowed (Figure 13~~Figure 13~~) and the higher average thermal efficiency obtained as well as electrical efficiency (Figure 14~~Figure 14~~), i.e. higher overall energy efficiency of the PV/T collector, because the lower PV/T temperature means lower heat loss and it is beneficial for electrical power generation. It is noted that, when there was a stagnation situation of the water loop with the water temperature inside the PV/T increasing while it was absorbing energy from the sun, the useful thermal efficiency was considered to be zero because there was no thermal energy carried out of the PV/T panel. The higher the set output temperature, the longer time it waited before the water pump started working. The moment when the water pump started, the average water temperature in the PV/T collector as a whole reached the targeted level as there was a nearly uniform temperature all over the collector in a stagnation condition. That led to the highest instantaneous useful thermal efficiency and a drop of instantaneous electrical efficiency, and this phenomenon is more obvious for the cases requiring higher temperature water output, e.g. 80 °C and 100 °C curves in Figure 14~~Figure 14~~. Once the water flowed and the fresh water at ambient temperature came into the absorber tubes, the average water temperature inside the PV/T collector dropped and the water flow rate in the next time step had to be adjusted lower accordingly to be able to deliver the targeted high temperature water output. Afterwards, the water flow rate increased again in the 40 °C and 60 °C curves as the increasing irradiance was intense enough to produce qualified water with relatively flat profile of thermal efficiency during the daytime; otherwise, for the 80 °C and 100 °C curves, the flow rate and the thermal efficiency decreased in a zig-zag pattern as the time went on.

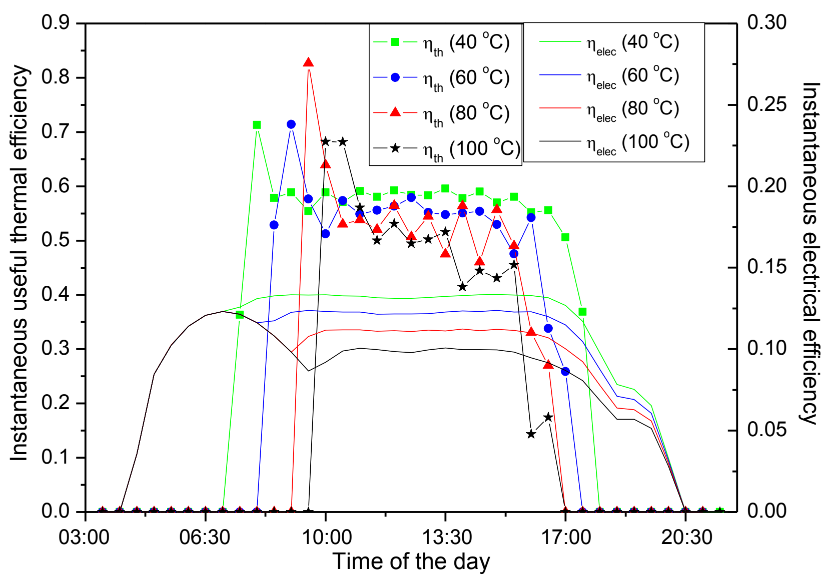

Figure 14. Instantaneous thermal efficiency and electrical efficiency of the PV/T collector with air gap.

The half-hourly variation profile of the water output temperature at different preset points for the PV/T collector without air gap (PV/T-no-AG) is shown in Figure 15~~Figure 15~~. It is not surprising to learn that under the given climatic condition, the water temperature of the PV/T-no-AG type cannot be heated higher than about 43 °C even in a stagnation condition all day long. The wind speed and ambient temperature can have considerable influence on the effective heat delivered, especially in the cold region even though in the sunny days the heat loss to the ambient could be much more compared to the PV/T-AG type. Therefore, it can be concluded that the addition of air insulation layer is significant to enhance thermal energy output of the PV/T collector especially for the weather conditions similar to that in Newcastle upon Tyne.

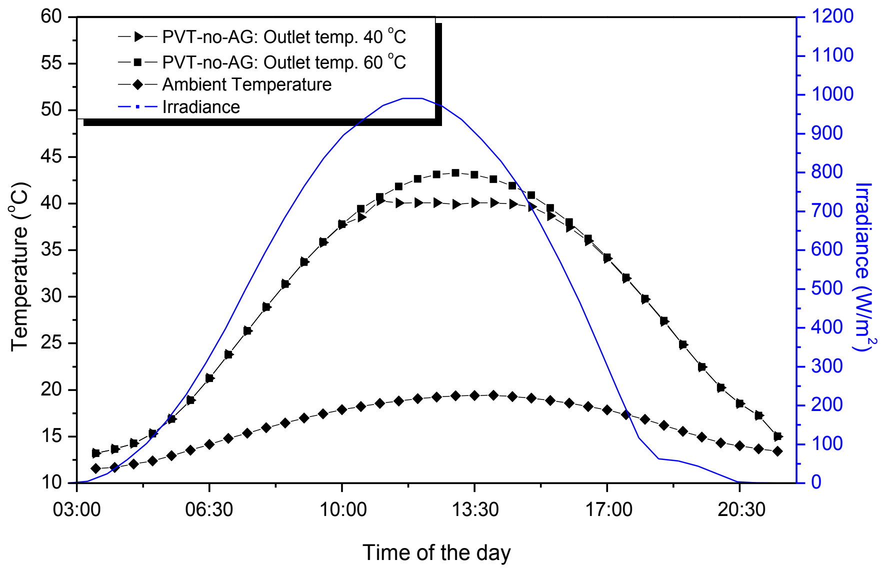

Figure 15. The water output temperature at different targeted levels from the PV/T without airgap collectors on a sunny summer day in Newcastle upon Tyne, UK.

Electrical power production from the PV/T-AG collector and PV/T-no-AG collector is shown in Figure 16~~Figure 16~~ in comparison with the production from the PV panel. The 40 °C curve of the PV/T-AG collector is closer to the reference PV curve, and has a slightly higher maximum power output during the mid-day than that of the reference PV curve; whereas, the electrical power gradually reduces with the increasing water output temperature, as the maximum power output on the 100 °C curve is about 23% lower than that of the reference PV curve. In general, the normal PV/T collector even without air gap design would be expected to produce more electrical power than the PV-only panel. However, in this work, the PV/T-no-AG collector operated under a stagnation condition of the water loop most of the time, which in fact to some extent hampered the heat dissipation and increased the PV cell temperature, as shown in Figure 15~~Figure 15~~. Because higher PV cell temperature has detrimental effect on electrical power generation, and the average PV cell temperature of the PV/T-no-AG collector is always higher than the reference PV panel, which explains the less production from the PV/T-no-AG collector than that of the reference PV panel. With the same reason, the power output curve of the reference PV panel is in between the 40 °C and 60 °C curves for the PV/T-AG collector, it is echoed by the comparison between the PV cell temperature curves in Figure 17~~Figure 17~~. It also implies that if the electrical generation is of primary, the PV cell temperature should be kept lower than 40 °C to have tangible improvement of electrical efficiency.

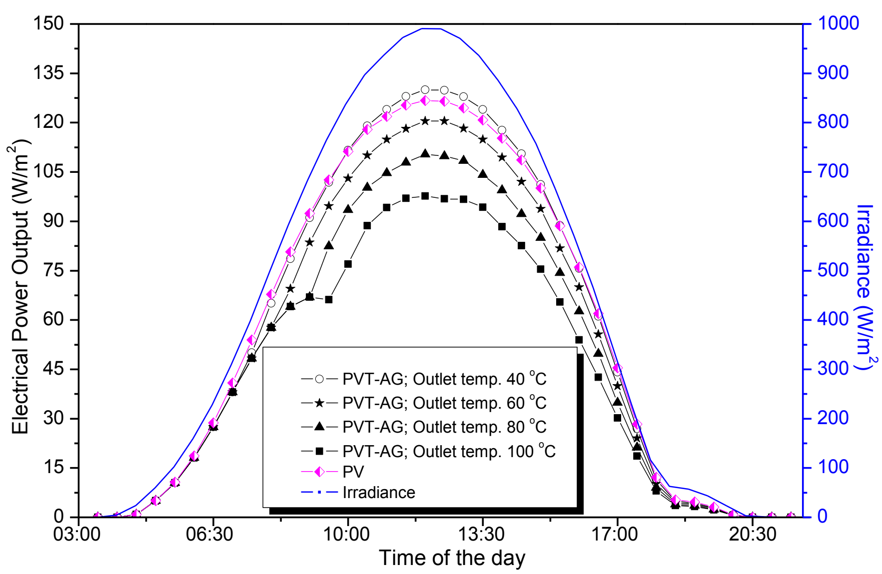

(a)

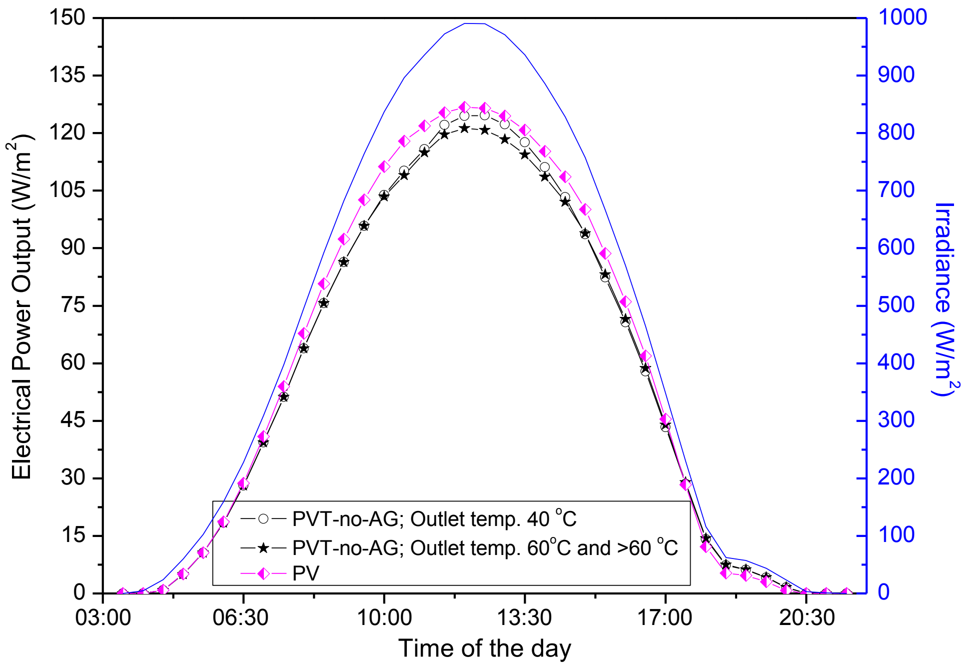

(b)

Figure 16. The electrical power output from (a) the PV/T with airgap; (b) the PV/T without airgap models on a sunny summer day in Newcastle upon Tyne, UK.

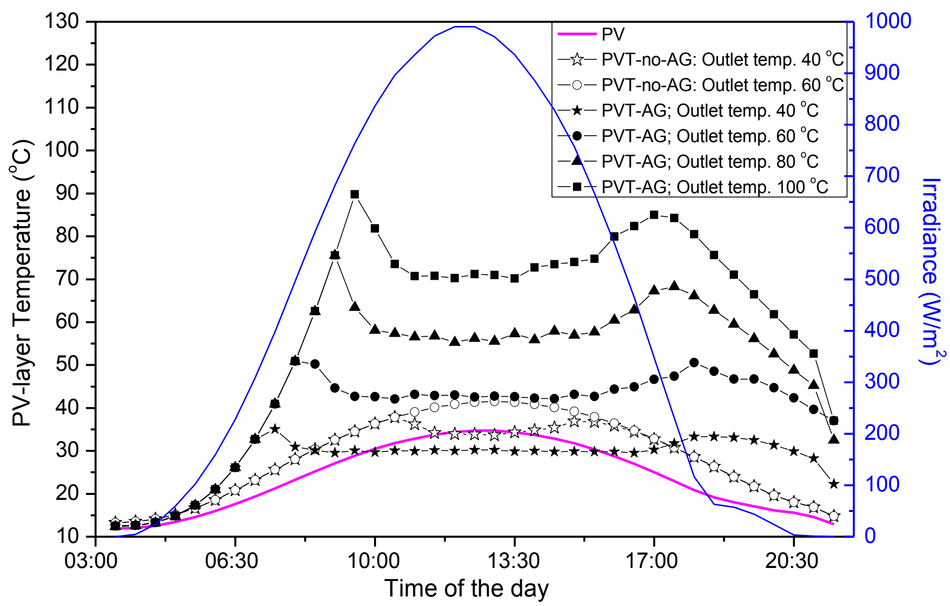

Figure 17. The PV-cell temperature of the PV/T collectors on a sunny summer day in Newcastle upon Tyne, UK.

4.3. Potential application integrated with thermal energy storage

(1) Domestic hot water use with water storage tank

For a typical UK household with approximately 30 m^2 rooftop area (a typical 4kWp of PV installation size) [62], the size of the PV/T-AG system installed at the optimum tilted angle was investigated to explore its potential of meeting the household hot water demand. The simulation results of the amount of water output at different temperature levels and the energy conversion efficiency by using the studied PV/T-AG collector was present in Table 4~~Table 4~~. On a typical sunny day in June in Newcastle, the amount of hot water production is from around 28 L/(day·m^2) to 133 L/(day·m^2) with the overall energy conversion efficiency from 45% to 66%, as the required output temperature ranging from 100 ºC to 40 ºC. For a sunny autunm day in September, the studied PV/T-AG collector can produce 19~98 L/(day·m^2) hot water depending on different required output temperature, with the overall energy conversion efficiency of 36%~59%, which is around 11%~18% lower than the efficiency obtained in summer.

Ref. [49] reported the mean daily hot water consumption of a single dwelling ranges from 98.44 litres in July to 133.16 litres in December in the UK. Table 5~~Table 5~~ lists the monthly usage in each month and the required installation area of PV/T-AG collector, based on the following consideration and assumption: the months of June and July are considered to have similar weather conditions, i.e. the simulation data for the month June is also used for performance calculation in July; while the spring and autumn months including August, September, October, March, April and May have similar weather conditions; the typical number of mostly sunny, partly sunny or clear days in Newcastle is 10 days each month, and the hot water is only produced during these days; the hot water is delivered at 60 ºC (i.e. the water outlet temperature); the water storage tank is assumed to have sufficient volume to store the solar thermal energy available for 10 days for the whole month usage; it is assumed to have negligible energy storage loss due to good insulation. Because of low irradiance, low ambient temperature and few sunshine hours during the winter time in Newcastle, the PV/T collector is not able to deliver useful thermal energy from November until February. Therefore, in order to satisfy the hot water demand from March to October with 100%

solar energy fraction, at least 7.76 m^2 of the PV/T-AG collector need to be installed for a single household. In the meantime, the total electricity output from March to October is around 500 kWh.

Table 4. Performance comparison between reference PV and PVT-AG collector under different conditions.

	Sunny summer day (28th June 2005)					Sunny autumn day (4th September 2005)				
Type of Model	$T_{w,o}$ (°C)	m_w (liter/day/ m^2)	Ave. η_{elec} (%)	Ave. η_{th} (%)	Total η (%)	$T_{w,o}$ (°C)	m_w (kg/day m^2)	Ave. η_{elec} (%)	Ave. η_{th} (%)	Total η (%)
PV	-	-	12.97	-	12.97	-	-	12.09	-	12.09
PVT with air gap	100.0	27.97	9.88	34.79	44.68	100.0	18.00	9.07	27.40	36.47
	80.0	42.00	10.96	40.40	51.36	80.0	28.45	10.76	33.54	44.30
	60.0	68.18	12.03	46.56	58.59	60.0	49.03	11.06	40.56	51.62
	40.0	132.87	12.99	53.22	66.21	40.0	97.78	11.98	46.82	58.80

(2) Integration with thermochemical sorption storage

The potential storage capacity of the thermochemical storage system is explored by exemplifying 30 m^2 installation area of the PV/T-AG collectors, when the hot water output is required to be at 100 °C. Table 5~~Table 5~~ lists the average monthly data of the operating conditions such as the water sources temperature and the ambient temperature as well as the required desorption temperature (T_{des}) with inclusion of the 5 °C equilibrium drop, which is only in the range of 79 °C to 87 °C. Therefore, the hot water temperature of 100 °C would be sufficiently high to make sure the proper desorption and energy charging process. The total amount of the solar heat that can be stored from March to October is around 3,522.55 GJ, which is adequate to cover the hot water demand of around 3,058.74 GJ [26] from November to February. In fact, the collector area can accordingly reduce to 26 m^2 but still fully meet the requirement. It is noted that zero energy loss has been assumed for the thermochemical sorption system, but the detailed design and analysis of the thermochemical sorption system is out of the scope of this work and will be presented in the future works.

Combined the results in the first application case for domestic hot water use in Table 5~~Table 5~~ and the electricity generation dada shown in Table 6~~Table 6~~, it can be expected that such an integrated system with 26 m^2 PV/T-AG collectors can fully satisfy the hot water demand of a single household all year around with 100% renewable sources, while the total solar electricity generation could be around 1365 kWh. In fact, the actual total annual electricity output could be higher than this value, because even in the deep winter when no useful hot water could be produced, there is still electricity output, but the simulation results presented in this work does not include the electricity generation in the winter time. It was reported that the average electricity consumption per British household without electric heating was around 3638 kWh [63]. That means at least half of the total electricity consumption can be met by renewable generation by using this integrated system.

Table 5. The potential performance of two applications of the PVT-AG collector

Month	T_{w_cold} (°C)	Avg. hot water consumption (m^3/month)	Hot water (60 °C) energy demand (GJ/month)	Required PV/T installation area for 60 °C hot water demand (m^2)	T_{amb} (°C)	T_{des} of $SrCl_2$(8/1) (°C)	Storable thermal energy (GJ/month) based on 30 m^2 installation area with $T_{w,o}$ = 100°C
Jan	9.62	3.62	760.60	-	3.0	-	0
Feb	9.32	3.49	739.56	-	3.1	-	0
Mar	10.70	3.90	817.23	7.76	5.1	74.13	521.85
Apr	13.70	3.44	670.35	6.86	7.1	75.88	478.09
May	15.32	3.81	722.47	7.59	9.9	78.32	417.08
Jun	17.26	3.50	629.80	5.01	13.0	80.99	525.48
Jul	19.33	3.05	515.19	4.37	14.5	82.28	477.09
Aug	18.67	3.27	566.56	6.52	14.4	82.19	320.31
Sep	17.88	3.38	598.07	6.73	12.6	80.65	358.82

Month	T_{w_cold} (°C)	Avg. hot water consumption (m^3/month)	Hot water (60 °C) energy demand (GJ/month)	Required PV/T installation area for 60 °C hot water demand (m^2)	T_{amb} (°C)	T_{des} of $SrCl_2$(8/1) (°C)	Storable thermal energy (GJ/month) based on 30 m^2 installation area with $T_{w,o}$ = 100°C
Oct	15.55	3.83	717.65	7.63	9.6	78.05	423.83
Nov	12.22	3.84	739.54	-	6.0	-	0
Dec	10.51	4.13	819.04	-	3.8	-	0

Table 6. Electricity output of the PVT-AG collector.

Outlet Temp. (°C)	Autumn & spring production (March, April, May, August, September, October)		Summer production (June, July)		Annual total (kWh)
	kWh/(m^2· day)	per 30m^2 PVT 60 days in total (kWh)	kWh/(m^2· day)	per 30m^2PVT 20 days in total (kWh)	
100	0.605	1089.0	0.810	486.0	1575.0
80	0.672	1209.6	0.899	539.4	1749.0
60	0.737	1326.6	0.987	592.2	1918.0
40	0.799	1438.2	1.066	639.6	2077.8

Considering the energy quality and the increasing electricity demand for wider electrification and electric vehicles, electricity may be still the primary desire for many households. The results generated in this work evidence the conflict between the electrical and thermal performance of the PV/T system, i.e. the electrical efficiency dropped from 12-13% to 9-10% if the heat output temperature was 40 °C compared with the case of 100 °C, namely, with the goal of fully covering the domestic hot water demand over a year, the electric output is depressed. Therefore, a trade-off between the electrical output and the temperature of heat output is needed depending on the end-user needs. To increase the electrical output, obviously the PV/T collector temperature has to be reduced. On the other hand, apart from the $SrCl_2$-NH_3 working pair, in fact there are countless number of reactive halide salts can be used in thermochemical sorption system to recover a wide temperature range of thermal energy, with great potential for various heating applications. For example, the $BaCl_2$-NH_3 working pair requires relatively lower desorption temperature than the $SrCl_2$-NH_3 pair, and its adsorption heat can be effectively used for low temperature heating facilities, e.g. floor heating or fan convector using 35 °C as feed temperature and 25 °C as return temperature, instead of high temperature heating considered in this work. Such an operating condition is more desirable for the purpose of improving electric efficiency and output. It would be worth more effort to evaluate the performance of thermochemical sorption systems using different working pairs with the optimal system configuration and suitable and effective applications for each working pair to explore the maximum potential of such an innovative integration.

There is another interesting integration to be explored further for more cost-effective and flexible utilisation of solar energy. The work [64] proposed and studied a novel integrated thermochemical sorption system combining a compressor/expander with a sorption cycle, and it can be driven by ultra-low grade heat (30~100 °C) for simultaneous electrical energy storage and thermal energy storage. During the energy charging process, the ultra-low grade heat is used for desorption with the aid of working fluid compression process powered by electricity through the compressor. In this case, both heat and electricity can be stored in form of chemical potential energy for long-term and zero-loss storage. During the energy discharging process, the stored energy can be used to flexibly deliver heating, or cooling, or electric output, depending on the end user demand. The most interesting point of the integration between this new sorption system and the PV/T system is, this sorption storage system can operate with high temperature heat input and small amount of electricity, or low temperature heat input with larger amount of electricity, which perfectly match with the performance characteristic of the PV/T system. Such a highly integrated system provides the desirable function equivalent to the combination of battery and thermal energy storage, and also maximises the flexibility of solar energy recovery and utilisation. In-depth investigation and detailed results of its potential performance will be reported in our next work.

5. Conclusion

This work numerically demonstrated the feasibility of the hybrid solar photovoltaic-thermal collector for domestic hot water application and the integration with thermochemical sorption system for seasonal energy storage. Instead of using the simplified model of electrical power generation in majority of research works on the PV/T collectors, a detailed model based on the one-diode model and the modified equations of R_{SH} and R_S were developed to couple with a CFD model for performance prediction of both thermal power and electrical power generation under various operating conditions.

The model validation suggests that the modified equations of R_{SH} and R_S proposed in this work as a function of irradiance and cell's temperature can improve the simulation accuracy under a wider range of operating conditions, especially for the cases with high PV cell temperature, compared to that resulted from assuming constant internal series resistances. The average error of the electrical power outputs at MPP can be considerably decreased from 3.57% to 0.85% for Siemens SM46 PV module operating at 60 °C, from 2.40% to 0.83% for Solarex MSX-60 module operating at 75 °C. In the meantime, the average error of the PV cell's temperature can be also improved to 0.63%.

Two types of PV/T collectors, with and without air gap, were simulated to see their performances under the high-latitude weather conditions, while the mass flow rate of the water loop was controlled and adjusted to obtain the hot water that leaves the PV/T collector at the targeted temperatures (from 60 to 100 °C) for specific applications. In Newcastle upon Tyne, to achieve the targeted heat output temperature of 60 °C in a sunny summer day based on 1 m^2 PV/T panel, the PV/T-AG collector has to operate at the HTF mass flow rate of lower than 0.175 kg/min and produces 68.18 litre/day/m^2 hot water with a thermal efficiency of around 47%, while the electrical efficiency is 12.03%, which is 0.94% lower than the PV panel. In contrast, the PV/T-no-AG collector produces heat output at no higher than about 43 °C under the same conditions.

Both thermal efficiency and electrical efficiency of the PV/T-AG collector is increased when it operates with lower outlet HTF temperature, because of less heat loss caused by the smaller temperature difference between the PV/T temperature and the ambient air and the positive effect of lower PV cell temperature on the electrical efficiency. The PV/T-AG can produce hot water at 100 °C in sunny summer days with lower total efficiency (44.68%) resulting from the high temperature of the panel leading to high heat loss and low electrical efficiency (9.88%). The comparative results suggest that the air-gap layer has significant effect to prevent massive heat loss especially in cold climate region where the ambient temperature is low almost all year round.

The application case studies demonstrated that (1) an installation of 7.76 m^2 air-gap PV/T collector can satisfy hot water demand (at 60 °C) of an ordinary single household in the city of Newcastle upon Tyne from March to

October; (2) integrated with an installation of 26 m^2 air-gap PV/T collector, the thermochemical sorption system using the working pair of $SrCl_2$-NH_3 can seasonally store and shift the heat load to cover the hot water demand from November to February. Such an integrated system can fully satisfy the hot water demand all year around and half of the annual electricity consumption for a single household. By taking the longevity of the collector into account, further studies on the life cycle analysis for high temperatures operation should be conducted.

Acknowledgement

The authors gratefully acknowledge the support from the Heat-STRESS project (EP/N02155X/1) and Centre for Energy Systems Integration (EP/P001173/1) funded by the Engineering and Physical Science Research Council.

References

[1] "Energy Storage: The Missing Link in the UK's Energy Commitments," Institution of Mechanical Engineers, London April 2014.

[2] A. H. A. Al-Waeli, K. Sopian, H. A. Kazem, and M. T. Chaichan, "Photovoltaic/Thermal (PV/T) systems: Status and future prospects," *Renewable and Sustainable Energy Reviews,* vol. 77, pp. 109-130, 2017.

[3] C. Babu and P. Ponnambalam, "The role of thermoelectric generators in the hybrid PV/T systems: A review," *Energy Conversion and Management,* vol. 151, pp. 368-385, 2017.

[4] Y. Tripanagnostopoulos, T. Nousia, M. Souliotis, and P. Yianoulis, "Hybrid photovoltaic/thermal solar systems," *Solar Energy,* vol. 72, pp. 217-234, 2002.

[5] V. Tomar, G. N. Tiwari, and T. S. Bhatti, "Performance of different photovoltaic-thermal (PVT) configurations integrated on prototype test cells: An experimental approach," *Energy Conversion and Management,* vol. 154, pp. 394-419, 2017.

[6] H. Zondag, D. de Vries, W. van Helden, R. van Zolingen, and A. A. van Steenhoven, "The yield of different combined PV-thermal collector designs," *Solar Energy,* vol. 74, pp. 253-269, 2003.

[7] B. M. Ziapour, V. Palideh, and M. Baygan, "Performance comparison of four passive types of photovoltaic–thermal systems," *Energy Conversion and Management,* vol. 88, pp. 732-738, 2014.

[8] M. Hazami, A. Riahi, F. Mehdaoui, O. Nouicer, and A. Farhat, "Energetic and exergetic performances analysis of a PV/T (photovoltaic thermal) solar system tested and simulated under to Tunisian (North Africa) climatic conditions," *Energy,* vol. 107, pp. 78-94, 2016.

[9] D. Su, Y. Jia, X. Huang, G. Alva, Y. Tang, and G. Fang, "Dynamic performance analysis of photovoltaic-thermal solar collector with dual channels for different fluids," *Energy Conversion and Management,* vol. 120, pp. 13-24, 2016.

[10] M. Y. Othman, S. A. Hamid, M. A. S. Tabook, K. Sopian, M. H. Roslan, and Z. Ibarahim, "Performance analysis of PV/T Combi with water and air heating system: An experimental study," *Renewable Energy,* vol. 86, pp. 716-722, 2016.

[11] K. E. Amori and H. M. Taqi Al-Najjar, "Analysis of thermal and electrical performance of a hybrid (PV/T) air based solar collector for Iraq," *Applied Energy,* vol. 98, pp. 384-395, 2012.

[12] F. Yazdanifard, M. Ameri, and E. Ebrahimnia-Bajestan, "Performance of nanofluid-based photovoltaic/thermal systems: A review," *Renewable and Sustainable Energy Reviews,* vol. 76, pp. 323-352, 2017.

[13] S. Hassani, R. Saidur, S. Mekhilef, and R. A. Taylor, "Environmental and exergy benefit of nanofluid-based hybrid PV/T systems," *Energy Conversion and Management,* vol. 123, pp. 431-444, 2016.

[14] A. H. A. Al-Waeli, K. Sopian, M. T. Chaichan, H. A. Kazem, H. A. Hasan, and A. N. Al-Shamani, "An experimental investigation of SiC nanofluid as a base-fluid for a photovoltaic thermal PV/T system," *Energy Conversion and Management,* vol. 142, pp. 547-558, 2017.

[15] M. Hosseinzadeh, A. Salari, M. Sardarabadi, and M. Passandideh-Fard, "Optimization and parametric analysis of a nanofluid based photovoltaic thermal system: 3D numerical model with experimental validation," *Energy Conversion and Management,* vol. 160, pp. 93-108, 2018.

[16] C. J. Smith, P. M. Forster, and R. Crook, "Global analysis of photovoltaic energy output enhanced by phase change material cooling," *Applied Energy,* vol. 126, pp. 21-28, 2014.

[17] Z. Qiu, X. Zhao, P. Li, X. Zhang, S. Ali, and J. Tan, "Theoretical investigation of the energy performance of a novel MPCM (Microencapsulated Phase Change Material) slurry based PV/T module," *Energy,* vol. 87, pp. 686-698, 2015.

[18] G. Feng, S. Liu, K. Huang, Y. Pan, and R. Niu, "Simulation for a New Type of Photovoltaic (PV) Fresh Air and Domestic Hot Water System," *Procedia Engineering,* vol. 121, pp. 1428-1434, 2015.

[19] A. Gaur, C. Ménézo, and S. Giroux--Julien, "Numerical studies on thermal and electrical performance of a fully wetted absorber PVT collector with PCM as a storage medium," *Renewable Energy,* vol. 109, pp. 168-187, 2017.

[20] A. H. A. Al-Waeli, K. Sopian, M. T. Chaichan, H. A. Kazem, A. Ibrahim, S. Mat*, et al.*, "Evaluation of the nanofluid and nano-PCM based photovoltaic thermal (PVT) system: An experimental study," *Energy Conversion and Management,* vol. 151, pp. 693-708, 2017.

[21] K. Touafek, A. Khelifa, and M. Adouane, "Theoretical and experimental study of sheet and tubes hybrid PVT collector," *Energy Conversion and Management,* vol. 80, pp. 71-77, 2014.

[22] T. T. Chow, A. L. S. Chan, K. F. Fong, Z. Lin, W. He, and J. Ji, "Annual performance of building-integrated photovoltaic/water-heating system for warm climate application," *Applied Energy*, vol. 86, pp. 689-696, 2009.

[23] M. Herrando, A. Ramos, J. Freeman, I. Zabalza, and C. N. Markides, "Technoeconomic modelling and optimisation of solar combined heat and power systems based on flat-box PVT collectors for domestic applications," *Energy Conversion and Management*, vol. 175, pp. 67-85, 2018.

[24] Y. Zhao, "Photovoltaic cell radiating and combined heat and power system," China Patent CN200820123998, 04 November, 2008.

[25] H. M. S. Hussein, "Theoretical and experimental investigation of wickless heat pipes flat plate solar collector with cross flow heat exchanger," *Energy Conversion and Management*, vol. 48, pp. 1266-1272, 2007.

[26] B. M. Ziapour and M. B. Khalili, "PVT type of the two-phase loop mini tube thermosyphon solar water heater," *Energy Conversion and Management*, vol. 129, pp. 54-61, 2016.

[27] A. Tiwari and M. S. Sodha, "Performance evaluation of hybrid PV/thermal water/air heating system: A parametric study," *Renewable Energy*, vol. 31, pp. 2460-2474, 2006.

[28] T. T. Chow, G. Pei, K. F. Fong, Z. Lin, A. L. S. Chan, and J. Ji, "Energy and exergy analysis of photovoltaic–thermal collector with and without glass cover," *Applied Energy*, vol. 86, pp. 310-316, 2009.

[29] R. Daghigh, M. H. Ruslan, A. Zaharim, and K. Sopian, "Effect of packing factor on the performance of PV/T water heater," in *International Conference on ENERGY & ENVIRONMENT, 6th*, 2011, pp. 304-309.

[30] M. Herrando, C. N. Markides, and K. Hellgardt, "A UK-based assessment of hybrid PV and solar-thermal systems for domestic heating and power: System performance," *Applied Energy*, vol. 122, pp. 288-309, 2014.

[31] T. Chow, "Photovoltaic-Thermal Collector System for Domestic Application," *Journal of Solar Energy Engineering (Transactions of the ASME)*, vol. 129, pp. 205-209, 2007.

[32] W. He, T.-T. Chow, J. Ji, J. Lu, G. Pei, and L.-S. Chan, "Hybrid photovoltaic and thermal solar-collector designed for natural circulation of water," *Applied Energy*, vol. 83, pp. 199-210, 2006.

[33] Z. Wang, J. Zhang, Z. Wang, W. Yang, and X. Zhao, "Experimental investigation of the performance of the novel HP-BIPV/T system for use in residential buildings," *Energy & Buildings*, vol. 130, pp. 295-308, 2016.

[34] H. Jouhara, J. Milko, J. Danielewicz, M. A. Sayegh, M. Szulgowska-Zgrzywa, J. B. Ramos, *et al.*, "The performance of a novel flat heat pipe based thermal and PV/T (photovoltaic and thermal systems) solar collector that can be used as an energy-active building envelope material," *Energy*, vol. 108, pp. 148-154, 2016.

[35] K. Vats, V. Tomar, and G. N. Tiwari, "Effect of packing factor on the performance of a building integrated semitransparent photovoltaic thermal (BISPVT) system with air duct," *Energy & Buildings*, vol. 53, pp. 159-165, 2012.

[36] H. M. S. Bahaidarah, A. A. B. Baloch, and P. Gandhidasan, "Uniform cooling of photovoltaic panels: A review," *Renewable and Sustainable Energy Reviews*, vol. 57, pp. 1520-1544, 2016.

[37] S. Dubey and G. N. Tiwari, "Analysis of PV/T flat plate water collectors connected in series," *Solar Energy*, vol. 83, pp. 1485-1498, 2009.

[38] A. Ibrahim, A. Fudholi, K. Sopian, M. Y. Othman, and M. H. Ruslan, "Efficiencies and improvement potential of building integrated photovoltaic thermal (BIPVT) system," *Energy Conversion and Management*, vol. 77, pp. 527-534, 2014.

[39] M. Rosa-Clot, P. Rosa-Clot, G. M. Tina, and C. Ventura, "Experimental photovoltaic-thermal Power Plants based on TESPI panel," *Solar Energy*, vol. 133, pp. 305-314, 2016.

[40] M. Hazami, F. Mehdaoui, N. Naili, M. Noro, R. Lazzarin, and A. Guizani, "Energetic, exergetic and economic analysis of an innovative Solar CombiSystem (SCS) producing thermal and electric energies: Application in residential and tertiary households," *Energy Conversion and Management*, vol. 140, pp. 36-50, 2017.

[41] N. Pardo García, G. Zubi, G. Pasaoglu, and R. Dufo-López, "Photovoltaic thermal hybrid solar collector and district heating configurations for a Central European multi-family house," *Energy Conversion and Management*, vol. 148, pp. 915-924, 2017.

[42] ~~H. Zondag, B. Kikkert, S. Smeding, R. de Boer, and M. Bakker, "Prototype thermochemical heat storage with open reactor system," *Applied Energy*, vol. 109, pp. 360-365, 2013.~~

~~[43] T. Li, R. Wang, and J. Kiplagat, "A Target-Oriented Solid-Gas Thermochemical Sorption Heat Transformer for Integrated Energy Storage and Energy Upgrade," *Aiche Journal*, vol. 59, pp. 1334-1347, 2013.~~

~~[44] F. Kuznik and K. Johannes, "A Review on Chemisorption Heat Storage in Low-energy Buildings," *Energy Procedia*, vol. 57, pp. 2333-2341, 2014.~~

~~[45] F. Kuznik, K. Johannes, and C. Obrecht, "Chemisorption heat storage in buildings: State-of-the-art and outlook," *Energy And Buildings*, vol. 106, pp. 183-191, 2015.~~

[46] N. Yu, R. Z. Wang, and L. W. Wang, "Sorption thermal storage for solar energy," *Progress in Energy and Combustion Science*, vol. 39, pp. 489-514, 2013.

[47] ~~K. E. N'tsoukpoe, H. Liu, N. Le Pierrès, and L. Luo, "A review on long-term sorption solar energy storage," *Renewable and Sustainable Energy Reviews*, vol. 13, pp. 2385-2396, 2009.~~

[48] P. Pinel, C. A. Cruickshank, I. Beausoleil-Morrison, and A. Wills, "A review of available methods for seasonal storage of solar thermal energy in residential applications," *Renewable and Sustainable Energy Reviews*, vol. 15, pp. 3341-3359, 2011.

[49] Z. Ma, H. Bao, and A. P. Roskilly, "Feasibility study of seasonal solar thermal energy storage in domestic dwellings in the UK," *Solar Energy,* vol. 162, pp. 489-499, 2018.

[50] O. Rejeb, H. Dhaou, and A. Jemni, "A numerical investigation of a photovoltaic thermal (PV/T) collector," *Renewable Energy,* vol. 77, pp. 43-50, 2015.

[51] P. Dupeyrat, C. Ménézo, M. Rommel, and H.-M. Henning, "Efficient single glazed flat plate photovoltaic–thermal hybrid collector for domestic hot water system," *Solar Energy,* vol. 85, pp. 1457-1468, 2011.

[52] V. Tyagi, S. C. Kaushik, and S. Tyagi, "Advancement in solar photovoltaic/thermal (PV/T) hybrid collector technology," in *Renew. Sust. Energ. Rev.* vol. 16, ed, 2012, pp. 1383-1398.

[53] H. S. Bao, R. G. Oliveira, R. Z. Wang, and L. W. Wang, "Choice of low temperature salt for a resorption refrigerator," *Industrial and Engineering Chemistry Research,* vol. 49, pp. 4897-4903, 2010.

[54] D. L. Evans, "Simplified method for predicting PV array output," *Solar Energy,* vol. - 27, pp. 555 - 560, 1981.

[55] V. J. Chin, Z. Salam, and K. Ishaque, "An accurate modelling of the two-diode model of PV module using a hybrid solution based on differential evolution," *Energy Conversion and Management,* vol. 124, pp. 42-50, 2016.

[56] H. F. Tsai and H. L. Tsai, "Implementation and verification of integrated thermal and electrical models for commercial PV modules," *Solar Energy,* vol. 86, pp. 654-665, 2012.

[57] C. Carrero, J. Amador, and S. Arnaltes, "A single procedure for helping PV designers to select silicon PV modules and evaluate the loss resistances," *Renewable Energy,* vol. 32, pp. 2579-2589, 2007.

[58] L. Adelard, F. Pignolet-Tardan, T. Mara, P. Lauret, F. Garde, and H. Boyer, "Sky temperature modelisation and applications in building simulation," *Renewable Energy,* vol. 15, pp. 418-430, 1998.

[59] A. Buck, "New equations for computing vapor pressure and enhancement factor," *Journal of Applied Meteorology, Boston,* vol. 20, pp. 1527-1532, 1981.

[60] K. Touafek, M. Haddadi, and A. Malek, "Design and modeling of a photovoltaic thermal collector for domestic air heating and electricity production," *Energy And Buildings,* vol. 59, pp. 21-28, 2013.

[61] *ANSYS Fluent Theory Guide Release 15.0*. Southpointe 275, Technology Drive, Canonsburg, PA 15317 2013.

[62] "Solar Energy Calculator Sizing Guide," E. S. Trust, Ed., ed, 2015.

[63] J.P. Zimmermann, M. Evans, J. Griggs, N. King, L. Harding, P. Roberts*, et al.*, "Household Electricity Survey: A study of domestic electrical product usage," R66141, May 2012.

[64] H. Bao, Z. Ma, and A. P. Roskilly, "Integrated chemisorption cycles for ultra-low grade heat recovery and thermo-electric energy storage and exploitation," *Applied Energy,* vol. 164, pp. 228-236, 2016.